Available online at www.sciencedirect.com
ScienceDirect
Trans. Nonferrous Met. Soc. China 35(2025) 3961−3984
Transactions of Nonferrous Metals Society of China
www.tnmsc.cn

Enhancing plasticity of metallic glasses via rejuvenation: A review

Quan DONG[1], Cai-ju LI[2], Baran SARAC[3], Jürgen ECKERT[3,4], Jun TAN[1]

1. College of Materials Science and Engineering, Chongqing University, Chongqing 400044, China;
2. Faculty of Materials Science and Engineering, Kunming University of Science and Technology, Kunming 650093, China;
3. Erich Schmid Institute of Materials Science, Austrian Academy of Sciences, Jahnstraße 12, A-8700, Leoben, Austria;
4. Department of Materials Science, Chair of Materials Physics, Montanuniversität Leoben, Jahnstraße 12, A-8700, Leoben, Austria

Received 22 April 2024; accepted 11 December 2024

Abstract: Recent attention has been directed towards tailoring the internal structure and enhancing the plasticity of metallic glasses (MGs) via rejuvenation treatments. This work aims to comprehensively review the various approaches and underlying mechanisms of inducing rejuvenation in MGs, including thermal-activated methods for deep-cooling cycling treatments and annealing-induced regeneration, mechanical-driven methods of pre-elastic loading and plastic deformation, thermo-mechanically coupled methods for thermo-mechanical creep and thermoplastic forming, and irradiation-induced rejuvenation. Additionally, strategies such as gradient rejuvenation for promoting a favorable distribution of free volume gradients to deflect shear bands are discussed for enhancing plasticity. Finally, the review delves into the challenges and prospects associated with advancing the development of MGs exhibiting high plasticity at ambient conditions. This review is anticipated to contribute to fostering a systematic understanding of the diverse methods and mechanisms employed to enhance the plasticity of MGs via rejuvenation treatments.
Key words: metallic glass; plasticity; rejuvenation; free volume; shear band

1 Introduction

Compared with traditional crystalline alloys, amorphous alloys, commonly referred to as metallic glasses (MGs), are characterized by rapid cooling from a supercooled liquid, resulting in a three-dimensional disordered arrangement of atoms. The unique atomic structure of MGs contributes to their exceptional mechanical, chemical, and physical properties, such as high strength [1−4], high hardness [1,5,6], corrosion resistance [7−9], high magnetic properties [10−12], and efficient catalysis [13−15], which have important application potential in the aerospace, military, and electric power industries, as well as in medicine, sports, catalysis, and other fields (see Fig. 1).

As we know, the deformation of MGs exhibits highly localized characteristics, that is, a large amount of plastic strain is concentrated in the shear band (SB) region with a thickness of only tens to hundreds of nanometers. Once the SB is generated, it is easy to expand, leading to the catastrophic fracture of the MG during deformation. MG exhibits typical room-temperature brittleness, one of the biggest problems hindering its development and applications [16]. For a long time, enhancing the plasticity of MGs has been the focus of researchers, who have made many efforts and attempts, such as customizing composition [17−19],

Corresponding author: Jun TAN, Tel: +86-23-65111520, E-mail: jun.tan@cqu.edu.cn
https://doi.org/10.1016/S1003-6326(25)66924-X

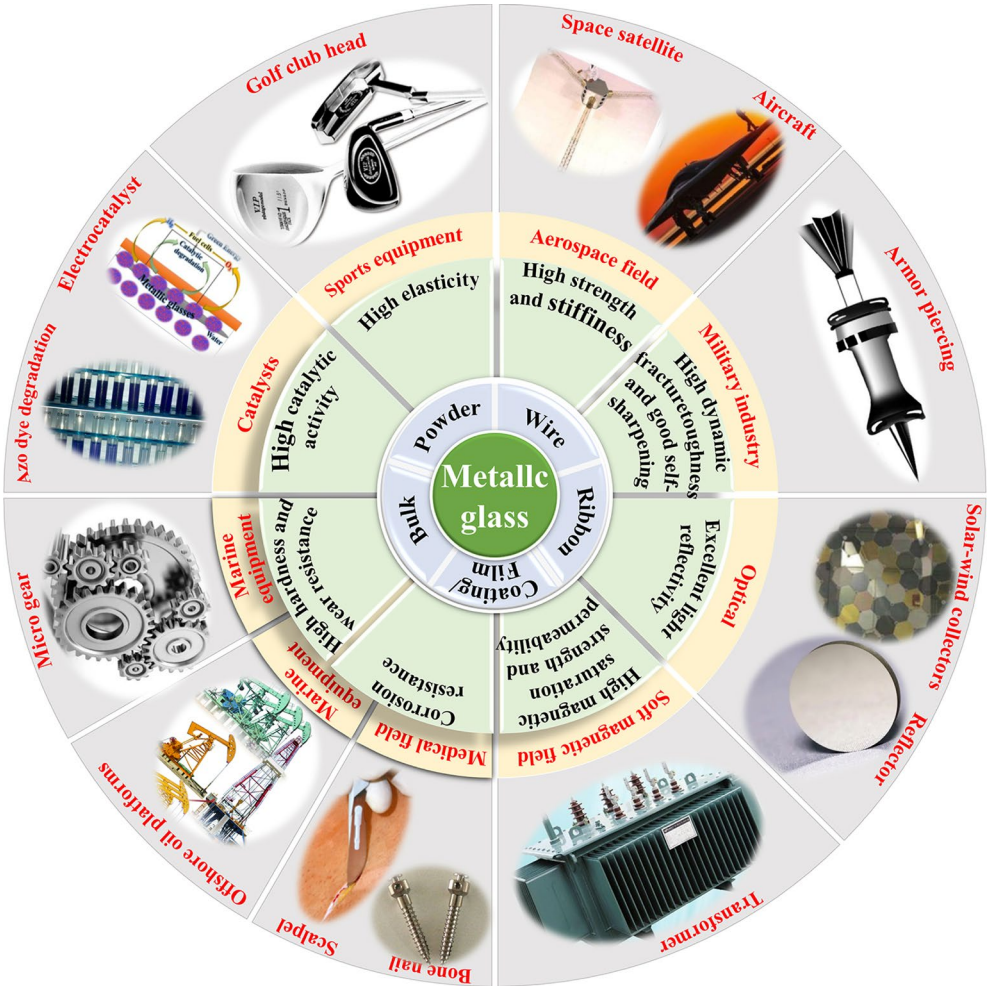

Fig. 1 Excellent properties and applications of MGs

adjusting Poisson ratio [20−23], controlling free volume [19,24−31], designing heterogeneous structures [32−34], tailoring stress states [25−40], and developing composite materials [41,42].

It is well known that MGs are metastable materials with different energy states under different preparation conditions. The process of changing from a high energy state to a low energy state is termed relaxation, whereas the process of changing from low energy to a high energy state is called rejuvenation. Figure 2 shows a schematic diagram of the rejuvenation and relaxation process of MGs [43]. In general, the more rejuvenated the bulk metallic glasses (BMGs), the larger the shear transition zone volume (Ω_{STZ}). The increase in Ω_{STZ} implies an increase in the average atomic spacing, and the BMG acquires a loose structure [25]. At the same time, the rejuvenation BMG in the higher energy state has more free volume (FV) and greater plasticity [44−47]. Many methods have been

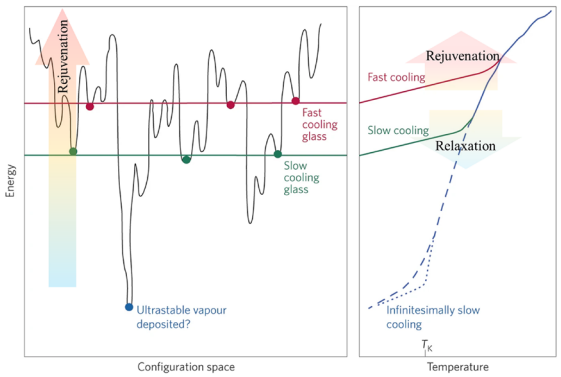

Fig. 2 Schematic diagram of rejuvenation and relaxation process in MGs [43]

attempted to promote the rejuvenation of MGs. To reach higher energy states, such as thermal-activated (e.g., deep cryogenic cycling treatment (DCT)) [26,27,48−53] and annealing-induced rejuvenation [44,54−58]), mechanical-drive (e.g., elastic preloading [52,59−64] and plastic deformation [46,65−71]), and thermo-mechanical

coupling (e.g., thermo-mechanical creep [45,72−75] and thermoplastic deformation [76−80]). Besides, irradiation can also promote local defect generation and atomic rearrangement, leading to the rejuvenation of MGs [30,81,82]. While the researchers proposed various methods and effects of rejuvenation on MGs, there is no specific review paper on enhancing plasticity via rejuvenation and will contribute to a systematic understanding of the diverse methods and mechanisms used to enhance the plasticity of MGs via rejuvenation treatments.

2 Thermal-activated approach for rejuvenation

2.1 Deep cryogenic cycling treatment

DCT can effectively improve the plasticity of BMGs [26,27,48−53,83,84]. Table 1 lists the thermal, physical, and mechanical properties of some Zr-based BMGs after DCT [25,28,29,48−50, 85−89]. After DCT, the relaxation enthalpy (ΔH_{rel}) upon heating of these Zr-based BMGs increases, the density decreases, and the plasticity of the BMGs increases. Compared with the as-cast BMG, the BMG after DCT has a higher SB population density in the vicinity [26], and the formation of a large number of SBs promotes the homogenization of the BMG deformation, resulting in increased plasticity. As shown in Fig. 3(a), the compressive plasticity of $Zr_{62}Cu_{24}Fe_5Al_9$ BMG increases from 4.9% to 7.6% after 60 cycles of DCT (DCT60). For MG composite, DCT does not affect the size and volume fraction of the second phase, and the increase in plasticity is only caused by the rejuvenation behavior of the amorphous matrix [50,90]. The Ta-rich $(Zr_{0.55}Cu_{0.3}Ni_{0.05}Al_{0.1})_{90}Ta_{10}$ BMGC exhibited up to 50.7% compressive plasticity under the combined action of matrix rejuvenation and the second phase after DCT [49].

It is well known that BMG is considered to be composed of a loosely packed core and a densely packed shell, and the core has a lower modulus and a higher coefficient of thermal expansion (CTE) than the shell [91]. DCT consists of two opposite effects: contraction caused by cooling and expansion caused by heating. Once the BMG is inserted into liquid nitrogen from boiling water, an instantaneous extensive temperature drop is imposed on the processed BMG, and vice versa. Under the stimulation of this instantaneous temperature gradient, the mismatched thermal expansion and contraction must be generated in the heterogeneous microstructure [92]. Consequently, the adjacent nanoscale regions will experience deformation incompatibility, inducing high local internal stress and inelastic strain [88]. The microscopic deformation of the core region by the internal stress may be equivalent to the macroscopic SB deformation of the external stress, causing the evolution of the core region and the increase of free volume (FV) [85]. Meanwhile, due to the faster response on the surface of the BMG than the interior during DCT, the sample temperature is spatially non-uniform during thermal cycling, which may cause a larger FV gradient. As shown in Fig. 3(c), α and β relaxations can occur in MGs at a temperature reaching 0.6 times the glass transition temperature (T_g). To avoid relaxation during thermal cycling, the upper limit temperature of DCT should be much lower than T_g, which is usually set at room temperature or boiling water temperature (Fig. 3(d)). While BIAN et al [93] investigated the temperature-dependent atomic structure evolution of $Zr_{64.13}Cu_{15.75}Ni_{10.12}Al_{10}$ MG using in-situ high-energy X-ray diffraction to explore the atomic origin for rejuvenation of a Zr-based MG at cryogenic temperature, and the results showed that interatomic distances shrank at cryogenic temperatures, and this shrinkage occurred in different atomic shells as the temperature decreased. The shrinkage was non-uniform, and at the same time, the shrinkage in the first shell caused thermal expansion in other regions.

After DCT, the sample is in a high-energy state (rejuvenated), introducing more FV and flow defects. As the number of cycles increases, the hardness of the samples decreases (insert in Fig. 3(b)), mainly due to the increase of flow defects in the samples after DCT. The flow defects of BMG are mainly related to its FV, and the increase of FV after DCT also promotes the formation of more soft regions. The SB-induced deformation process of BMG is mainly coordinated by the defect assistance. The defects here can be thought of as liquid-like regions of loosely packed atoms. On the one hand, a high content of defects can significantly promote the initiation of SB. On the other hand, the propagation of SB has a greater probability through defect regions with higher

Table 1 ΔH_{rel}, density (ρ), and plastic strain (ε_p) of DCTed Zr-based BMGs

BMG	Temperature range	Cycle	ΔH_{rel}/(J·g^{-1})	ρ/(g·cm^{-3})	ε_p/%	Ref.
$Zr_{52.5}Cu_{17.9}Ni_{14.6}Al_{10}Ti_5$	77 K→373 K	0			8.00	[25]
		100			28.00	
$Zr_{59.5}Nb_{4.8}Cu_{14.4}Ni_{11.6}Al_{9.7}$	77 K→373 K→RT	0	~11.450		~0.91	[28]
		10	~12.150		~1.17	
		20	~13.180		~2.13	
		30	~12.340		~1.28	
		40	~11.580		~0.90	
$Zr_{55}Cu_{30}Al_5Ni_{10}$	220 K→RT	30		6.8195	6.50	[29]
	180 K→RT	30		6.8184	7.50	
	140 K→RT	30		6.8174	9.80	
$Zr_{46}Cu_{46}Al_8$	108 K→RT	0	5.451		0.22	[48]
		10	9.356		0.50	
		20	8.053		0.82	
		60	7.033		2.02	
$(Zr_{0.55}Cu_{0.3}Ni_{0.05}Al_{0.1})_{99}Ta_1$	108 K→RT	0	13.600	6.8290	4.40	[49]
		30	15.700	6.8200	12.50	
$(Zr_{0.55}Cu_{0.3}Ni_{0.05}Al_{0.1})_{97}Ta_3$	108 K→RT	0	9.200	6.8370	5.60	[49]
		30	10.800	6.8270	13.10	
$(Zr_{0.55}Cu_{0.3}Ni_{0.05}Al_{0.1})_{95}Ta_5$	108 K→RT	0	10.800	6.8460	9.00	[49]
		30	12.800	6.8360	14.40	
$(Zr_{0.55}Cu_{0.3}Ni_{0.05}Al_{0.1})_{93}Ta_7$	105 K→RT	0	10.300	7.689 0	20.70	[50]
		30	12.200	7.6750	27.20	
$(Zr_{0.55}Cu_{0.3}Ni_{0.05}Al_{0.1})_{91}Ta_9$	105 K→RT	0	10.900	7.9280	32.80	[50]
		30	13.300	7.9070	37.80	
$(Zr_{0.55}Cu_{0.3}Ni_{0.05}Al_{0.1})_{90}Ta_{10}$	105 K→RT	0	10.600	7.9680	43.50	[50]
		30	13.100	7.9430	50.70	
$Zr_{55}Cu_{30}Al_{10}Ni_5$	180 K→RT	0	12.700	6.8243	4.00	[85]
		30	14.600	6.8162	11.00	
$Zr_{55}Al_{10}Ni_5Cu_{29}Y_1$	77 K→373 K	0	0.840		0.570	[86]
		20	1.230		1.16	
		40	1.510		1.40	
		60	2.140		1.98	
TiZrHfBeCu	77 K→RT	0			0.62	[87]
		5			2.10	
		10			3.11	
		15			3.64	
		20			5.38	
$Ti_{20}Zr_{20}Hf_{20}Be_{20}Cu_{7.5}Ni_{12.5}$	77 K→373 K	0			0.60	[88]
		15			2.90	
		30			3.40	
		60			4.20	
		90			4.40	
		120			4.60	
		240			5.20	
$Zr_{55}Cu_{30}Ni_5Al_{10}$	77 K→343 K	0			2.10	[89]
		40			8.30	

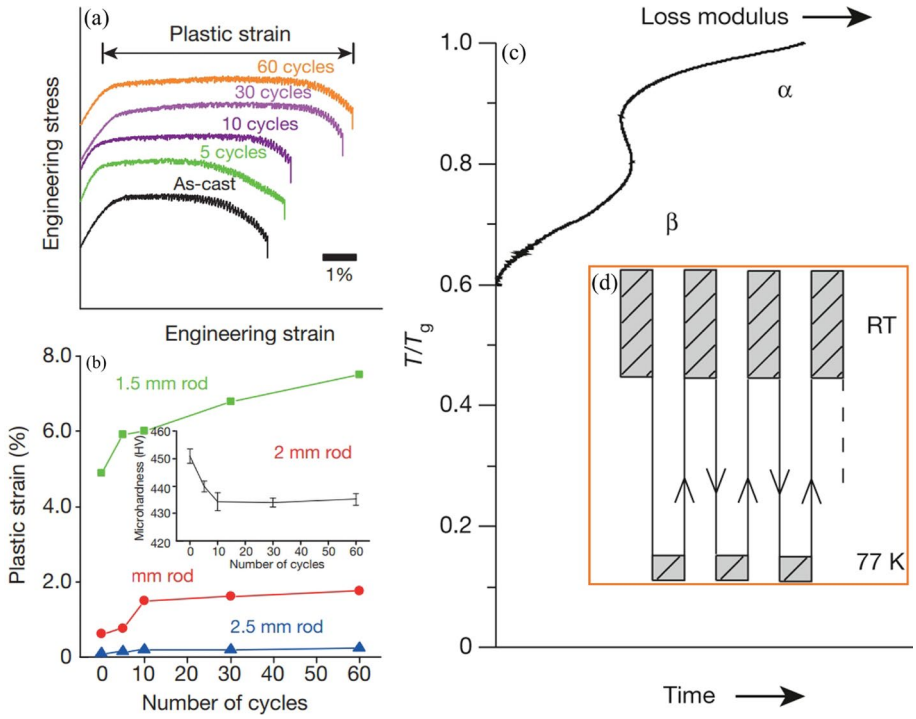

Fig. 3 (a) Stress−strain curves of $Zr_{62}Cu_{24}Fe_5Al_9$ of DCTed BMGs; (b) Plastic strain of $Cu_{46}Zr_{46}Al_7Gd_1$ BMG in different states after DCT; (c) Loss modulus as function of T/T_g; (d) Samples cycled from near room temperature to liquid-nitrogen temperature [26]

defect density. After DTC treatment, the defect density in the BMG increases, eventually enhancing the plasticity of BMG. The plasticity and defect density of the BMG are modelable by the percolation theory of composites [94]:

$$\varepsilon_p \propto (V_d^c - V_d)^{-\beta} \quad (1)$$

where V_d^c is the percolation threshold or the critical defect volume fraction to form local shear transition zone (STZ) percolation around the defect site, V_d is the volume fraction of the defect site, and β is a power exponent. In two-phase composites, the percolation threshold depends on the morphology and size of the second phase and the size ratio of the constituent phases [95−97]. The volume fraction (V_d) of defect points is not only related to defect density (i.e., the number of defect points or the average interval λ between defect points in Fig. 4) but also related to the characteristic volume (determined by the average diameter d of defects in Fig. 4) of defects. Therefore, the value of d/λ will be a key parameter for the occurrence of local percolation in STZ around the defect site. d is considered the geometric barrier for the STZ around the defect to penetrate the matrix, and λ represents the mean free path of STZ acceleration or development towards SB around the defect [48]. As shown in Fig. 4, compared with the as-cast BMG, the BMG after DCT has a larger defect density and a smaller activation volume.

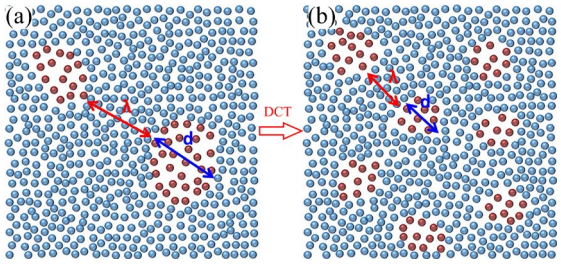

Fig. 4 Schematic illustration of local configuration of BMGs with different defect densities and defect activation volume before (a) and after (b) proper DCTs [48]

The rejuvenation effect of DCT is affected by the internal heterogeneity before DCT [26,98,99], the number of cycles [25,28,48,87,88], and the low limit temperature [29]. Firstly, as shown in Fig. 3(c), the less initial FV inside the BMG (large casting size or incomplete annealing) results in poor rejuvenation. Once the heterogeneity or FV is eliminated (fully annealing), DCT becomes

ineffective and cannot rejuvenate the BMG [26,99]. Secondly, lower temperature during cycling can restore the glass to a higher energy state due to higher internal stress [29]. At the same time, the plasticity of most BMGs increases with the number of cycles. For BMGs of the same composition, Ω_{STZ} increases as the number of DCT cycles increases, and a larger Ω_{STZ} is beneficial to creating multiple SBs, resulting in larger plastic deformation [100]. For example, the Ω_{STZ} of $Zr_{55}Al_{10}Ni_5Cu_{29}Y_1$ BMG after 60 DCT cycles (DCT60) increased from as-cast 1.28 to 2.83 nm^3, and the increase in plasticity was about four times [86]. However, when the number of cycles exceeds a certain amount, the plasticity does not increase but decreases [28,51,101]. ZHU et al [28] claimed that since atoms with high mobility occupied the extra space of the initial icosahedron, the internal stress activated the soft regions and the icosahedron with relatively low mobility of atoms acted as a hard region, impeding the soft zone movement. Therefore, the internal stress of the icosahedron is raised to a high level, and the proliferation of the icosahedral short-range ordered structure leads to a decrease in plasticity.

Not all BMGs show apparent rejuvenation behavior after DCT, and BMG rejuvenation behavior is affected by the system's fragility. For example, WAN et al [102] suggested that the plasticity of MGs is positively correlated with the fragility (m) of the supercooled liquid (Fig. 5(a)), i.e., MGs with greater fragility exhibit higher plasticity, and plasticity−fragility satisfies the following relationship:

$$\varepsilon_p = 92\exp[-73/(m-15)] \quad (2)$$

As shown in Fig. 5(b), for the same MG system, when the same rejuvenation means are applied, the degree of BMG rejuvenation is positively correlated with the magnitude of fragility, and MGs formed from stronger fluids tend to be more rejuvenated [71]. Some loosely packed regions are embedded in the densely packed matrix, and the FV is locked by surrounding atoms. A BMG with a higher fragility means a more stable amorphous structure. Therefore, relative to the strong BMG with a low fragility, the fragile BMG with a high fragility requires more activation energy to grow the cage for a certain distance, which makes it more difficult to induce excessive FV and rejuvenation [87,103,104]. As PENG et al [51] found that, Vit1 BMGs with high fragility (47−50) and high glass forming ability (GFA) exhibited insignificant rejuvenation behavior and limited improvement in plasticity after DCT. However, it is important to note that the degree of MG rejuvenation varies considerably for different MG systems or by imposing different means of rejuvenation. It can be seen from Fig. 5(b) that compared with other BMG systems, the rejuvenation effect of Zr-based BMG is more sensitive to fragility. That is, a small change in the fragility can cause a large change in ΔH_{rel}. Obviously, for Zr-based BMG, it is particularly important to pay attention to its fragility.

DCT has the advantages of being non-destructive, simple to operate, and highly rejuvenating. Furthermore, it should be recognized that DCT-induced rejuvenation has a memory for the original state of MG, i.e., the ΔH_{rel} value will relax to that of the casting state after DCT has been stopped and held at room temperature (RT) for some time [105].

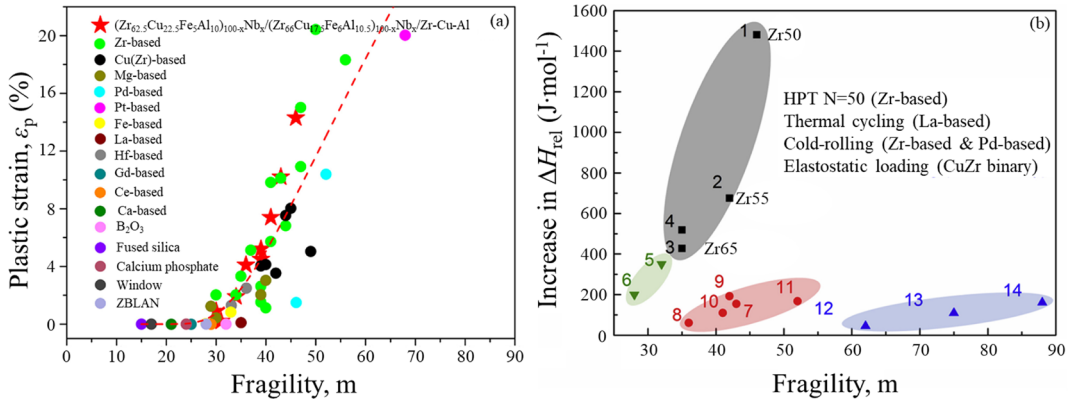

Fig. 5 (a) Plastic strain vs fragility near supercooling region reported for some glasses [102]; (b) ΔH_{rel} obtained by various rejuvenation methods vs fragility of processed samples [71]

2.2 Annealing-induced rejuvenation

Pure thermal rejuvenation can also achieve high-energy state transitions of BMGs [44,54−58]. Annealing temperature [106,107] and cooling rate after isothermal [44,56,108,109] are important factors affecting pure thermal rejuvenation. The thermal rejuvenation procedure for MG entails a sequence of steps, including swift heating, maintaining a steady temperature at an annealing point (T_a) that exceeds the glass transition temperature (T_g), and rapid quenching with a high cooling rate. A higher cooling rate after isothermal annealing in rejuvenation annealing than that in the initial quenching process is necessary for thermal revival, and thermal tempering can only be achieved when T_a is above a certain critical temperature (T_c). The former is required to suppress relaxation during quenching, while the latter is required to achieve high-energy states [56,57,110]. The T_c levels of BMG in different systems are different, but all require T_c be higher than T_g. Figure 6 shows a schematic diagram of the energy/volume changes in the initial melt quenching (A→D) and the subsequent thermal loading process (D→G) to explain the thermal loading conditions required for thermal rejuvenation: (1) T_a is much higher than a certain critical temperature T_c ($T_a \gg T_c$), and then the amorphous metal may rapidly relax to an equilibrium liquid state during the heating phase before the annealing process begins (green curve in Fig. 6). As the equilibrium liquid is cooled (F→G), sooner or later, the liquid will deviate from the equilibrium liquid, and the final structure will freeze into the glass. The cooling rate of annealing (R_q^i) > melt-quench cooling rate ($\tilde{R}_q$) induces an earlier deviation from the equilibrium liquid state and leads to higher energy/volume regenerated glass (red curves in Figs. 6(a) and (b)), while $R_q^i < \tilde{R}_q$ leads to MG aging (blue curve in Fig. 6(c)). (2) $T_a > T_c$, then the annealing time (t_a) becomes a key factor in addition to the cooling rate, because the relaxation time to reach the equilibrium liquid is longer compared with the heating and annealing time. As shown in Fig. 6(b), a longer annealing time leads to a larger energy/volume increase during isothermal annealing and eventually motivates the rejuvenation of the cooled glass (solid red curve), while a shorter annealing time may cause glass aging (red dashed curve). Therefore, there is a critical minimum annealing time (t_c) when T_a is low, and rejuvenation can only be achieved if $t_a > t_c$. (3) As shown in Fig. 6(d), if $T_a < T_c$, the annealing process always leads to the aging of the MG without rejuvenation.

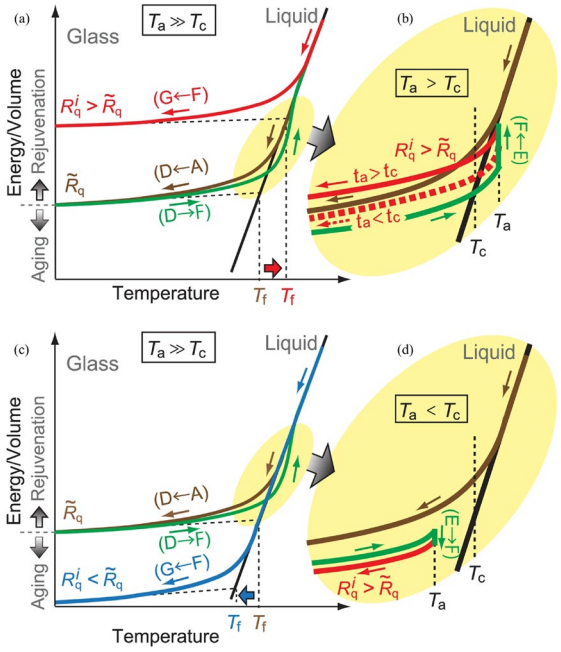

Fig. 6 Schematic of energy/volume change during thermal loading processes: (a) $T_a \gg T_c$ and $R_q^i > \tilde{R}_q$; (b) $T_a > T_c$ and $R_q^i > \tilde{R}_q$; (c) $T_a \gg T_c$ and $R_q^i < \tilde{R}_q$; (d) $T_a < T_c$ and $R_q^i > \tilde{R}_q$ [56]

Rapid annealing (flash annealing) can heat the BMG to a higher temperature than T_g in a relatively short time (millisecond level) [55], driving the BMG to a higher energy state. Currently, means to achieve rapid heating include resistive Joule heating with high-density current [111−114], electrical pulses [111−114] and capacity-discharge [115−117], and induction heating [118−120] and infrared heating [121], etc. Joule heating is widely used because there is no skin effect like induction heating but overall heating.

Flash annealing and subsequent rapid quenching can input energy to the MG, which can manipulate its energy state. MG can relax or rejuvenate in different energy states by controlling the temperature of flash annealing. Annealing in the supercooled liquid region (SLR) decreases the volume fraction of crystal-like ordered (CLO) regions or SLRs, and the MG is reactivated and placed in a high-energy state. However, flash annealing of MGs below T_g typically undergoes

relaxation, leading to embrittlement [122]. In particular, electrical pulse treatment (EPT) utilizes resistive Joule heating, where the electrons dissipate part of the electrical energy as heat, rapidly heating the BMG [114]. BMGs are heated above T_g into a state with increased enthalpy and heterogeneity within milliseconds, and then snap-frozen to suppress relaxation and maintain disordered structures [55]. In addition, part of the electrical energy can transfer momentum to atoms through electron bombardment, creating electromigration (EM) force. Electron scattering forces or electron winds prompt EM to promote atomic diffusion in the direction of electron transport [123−125]. Electrical pulses can accelerate FV motion, achieve plastic forming and tailor mechanical properties [126−128]. The synergistic effect of rapid heating and cooling and the enhancement of atomic mobility may contribute to the rejuvenation of BMGs [112]. Due to the unique EM contribution, even the annealing temperature of EPT is slightly lower than T_g to promote rejuvenation [114]. However, it has also been reported that EPT significantly accelerates relaxation or crystallization, so embrittlement occurs [127].

Understanding the synergistic effect of annealing temperature and time on the embrittlement of MG is key to tailoring the properties through heat treatment. KUMAR et al [129] investigated the time−temperature relationship between thermal relaxation and embrittlement of MGs. As shown in Fig. 7, a processing window exists at a high temperature and short processing time, so annealing does not induce brittleness in this regime. The window is divided into ductile and brittle regions by the brittleness curve. Brittleness below T_g is associated with structural relaxation, and the difference between embrittlement and relaxation time narrows with increasing temperature. In the annealing process of $T_a \geq T_g$, because the relaxation time is very short (10^2−10^{-2} s), it is not related to the embrittlement kinetics, which is related to the crystallization time. It is generally annealed at a high temperature and in a short time for thermal rejuvenation, which can well avoid the embrittlement curve.

Although the recovery annealing technique opens up a new path for regulating the energy state of MGs, the requirement for an extremely high cooling rate presents considerable challenges in practical applications, especially when treating large-sized BMGs.

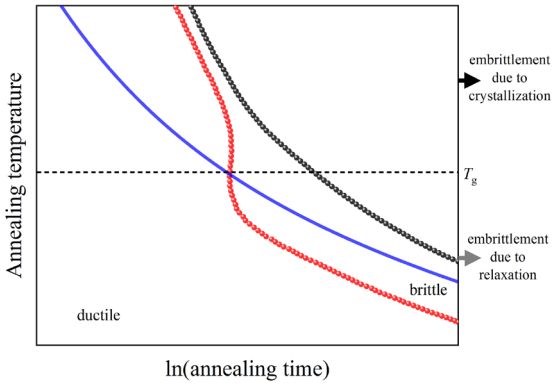

Fig. 7 Schematic illustration of embrittlement in BMG originating from relaxation and crystallization [129]

3 Mechanical-driven rejuvenation

3.1 Pre-elastic deformation

3.1.1 Elastostatic loading

Pre-elastic deformation is one of the techniques to improve the rejuvenation of BMG [52,59−64,130], and no SB is formed during the rejuvenation. MG slowly undergoes irreversible non-affine deformation under loads (σ_l) below the yield stress (σ_y) for a long time, leading to the rejuvenation of the structure. The main mechanism for pre-elastic deformation-induced rejuvenation is considered to be volume expansion caused by an increase in the average atomic bond length [64]. Table 2 lists the ΔH_{rel} and ε_p of some Zr-based BMGs after elastic precompression [59,61,62,64, 131−133]. The rejuvenation effect of elastic preloading is affected by compressive load and loading time. Rejuvenation in elastic pre-compression mode requires a critical load value [134,135]. As shown in Fig. 8(a), when loading at a stress P below σ_y, coalescence of the loosely packed and densely packed regions may occur (i.e., coalescence of negative and positive FV), resulting in volume shrinkage and permanent deformation, as indicated by the decrease in loose and the increase in density of elastically compressed BMGs, stress-driven coagulation of loose and dense regions will contribute to the uniform deformation of MGs at ambient temperature. This stress-induced FV annihilation is also called the mechanical annealing effect [134]. Once the applied stress is higher than the yield stress, the shear expansion will lead to the

Table 2 Some events of pre-elastic loading promoting rejuvenation of Zr-based BMGs

BMG	(σ_l/σ_y)/%	Loading time/h	ΔH_{rel}/(J·g^{-1})	ε_p/%	Ref.
$Zr_{55}Cu_{30}Ni_5Al_{10}$	0*	24		1.90	[59]
	5*	24		2.70	
	10*	24		4.30	
	15*	24		6.80	
	20*	24		7.20	
$Cu_{50}Zr_{50}$	90	0	4.700	4.00	[61]
		12	5.260	4.40	
$Zr_{46}Cu_{46}Al_8$	0	2		~0	[62]
	28	2		0.20	
	56	2		~0.50	
	84	2		~1.00	
$Zr_{55}Cu_{30}Al_{10}Ni_5$	0	24	6.200	3.75	[64]
	40	24	7.460	4.12	
	70	24	9.710	4.47	
	80	24	11.630	5.29	
	90	24	13.200	8.97	
Aged $Zr_{64.13}Cu_{15.75}Ni_{10.12}Al_{10}$	60**	0		27.30	[131]
		1		39.40	
$Zr_{64.13}Cu_{15.75}Ni_{10.12}Al_{10}$	0	0	4.840	2.50	[132]
Aged $Zr_{64.13}Cu_{15.75}Ni_{10.12}Al_{10}$	60**	0	2.190	1.60	[132]
		1	3.280	3.50	
		4	2.430	~0	
$Zr_{48}Cu_{36}Al_8Ag_8$	0	0	5.833	2.80	[133]
	~20	60		4.30	
	~40	60	6.141	4.60	
	~80	30	6.197	6.70	
	~80	60	5.499	1.90	
	~80	120		0.70	

*: Tensile load; **: Lateral load; Others: Compressive load

generation of FV, i.e., the structural rejuvenation of the BMG, as shown in Fig. 8(b). There is a certain critical stress (σ_c) that divides relaxation and rejuvenation, which is about 70% of σ_y, and only at pressures above σ_c does the effect of stress lead to the rejuvenation of the BMG. Figure 8(c) shows a schematic diagram of the transition from mechanical relaxation to rejuvenation. When the stress is lower than the σ_c, the effect of stress will accelerate the aging, that is, mechanical relaxation, otherwise, the stress effect will rejuvenate the amorphous structure. When the stress is above σ_y, plastic flow begins [136].

The holding time of elastostatic loading also significantly affects the rejuvenation effect of MG. CUI et al [137] found that after applying a constant load with $0.87\sigma_y$ to Vit1 MG, the MG underwent rejuvenation and relaxation successively with increased holding time. In the early stage of load application, the ΔH_{rel} and FV of MG increased with holding time, more defects with larger sizes were activated, and the compressive plasticity was also increased from 1.4% to 3.4% of the as-cast alloy after holding for 40 h. Further, after increasing the holding time to 60 h, the MG undergoes a relaxation transition, and the plasticity decreases significantly.

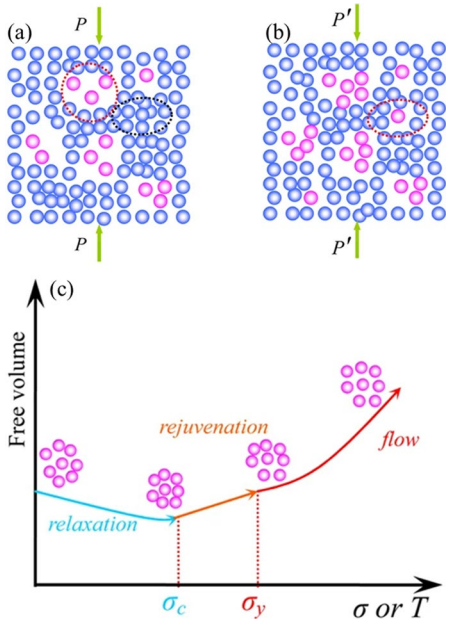

Fig. 8 Schematic diagrams of LLRs and SLRs at above (a) and below (b) yield stress, and mechanical relaxation to rejuvenation transition (c) [136]

Notably, the pre-elastic deformation technique typically requires a longer loading time to achieve a high-level regeneration effect, resulting in a higher time cost for processing.

3.1.2 Cyclic elastic loading

In recent years, cyclic elastic loading via mechanical cycling to induce rejuvenation has also received increasing attention [138−140]. When the MG is subjected to cyclic load within the elastic limit, the stress also causes local non-affine atomic displacements, i.e., the atoms undergo jumping. The jumped atoms with potential energy higher than the original state introduce FVs and flow defects, leading to a rejuvenation process. This rejuvenation increases atomic disorder, which puts the atomic arrangement in a more unstable state [139]. YE et al [141] suggested that the softening behavior of cyclic elastic loading was related to the activation of string-like liquid sites and atomic bond breaking in the glass structure. ZHANG et al [138] suggested that the coupling of thermal activation and stress led to most flow defects being excitedly activated through collective rearrangement. The density of the liquid-like flow defects, potential energy, and fictive temperature increased (Fig. 9(c)). Furthermore, the intensity of the β relaxation peaks originating from flow defects increased and shifted to the low activation energy side after rejuvenation, and their relaxation time distributions were more extensive, as shown in Fig. 9(a).

Compared with elastostatic loading, the range of adjustment under cyclic loading is relatively large, including the number of cycles [142], stress amplitude [138], stress rate [138], mean stress [138,143], and frequency [140], etc. Generally, the

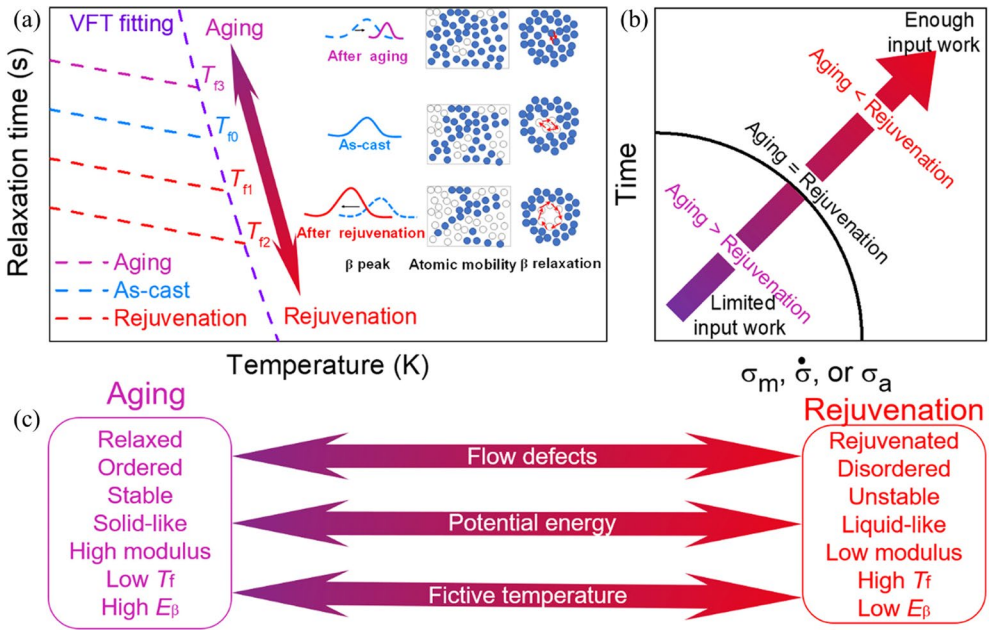

Fig. 9 (a) Evolution of relaxation time with temperature for MGs accompanied by different energy states (Inset shows the evolution of relaxation and atomic mobility with aging or rejuvenation); (b) Competitive behavior of aged and rejuvenated MGs during mechanical cycling; (c) Indicators of rejuvenation and aging behavior of MGs [138]

balance between structural relaxation and deformation-induced structural recovery depends on various factors, mainly the mechanical cyclic strength, including stress amplitude, stress rate, and mean stress. Moreover, there exists a threshold value for the mechanical cycling strength, and only if the threshold value is exceeded can additional thermal/mechanical energy input to the MGs compensate for and exceed the enthalpy lost in the structural relaxation process, thus realizing an improvement in the energy state of the MGs (Fig. 9(b)). LI et al [142] suggested that there was also a critical value for the number of cycles, below which the potential energy increased with the number of cycles, and rejuvenation saturated when the critical value was reached.

Ultrasonic vibration [144−147] is also an important cyclic loading method for inducing rejuvenation of MG. The rejuvenation of conventional pre-elastic compression takes a long time, and reverse relaxation intervention is inevitable during this time-consuming process, thereby mitigating the effect of rejuvenation. In contrast, ultrasonic vibration largely avoids time-varying structural relaxation and crystallization [146]. Ultrasonic vibration pre-compression can achieve the rejuvenation of Zr-based BMGs in a short time, improving ΔH_{rel} and plasticity [144−146]. First, the high-frequency strain energy is converted into heat/internal energy. The combined effects of externally applied elastic stress, internally converted heat, and ultrasonic vibration resonance of the atoms promote the acquisition of more loose atoms while introducing more FV into the structure of the BMG [145,147,148]. Ultrasonic amplitude and prestress/prestrain are the main factors affecting the rejuvenation effect of ultrasonic vibration preload. With the increase of ultrasonic amplitude or pre-pressure, ΔH_{rel} of BMG increases, indicating a significant rejuvenation effect [144−146]. LI et al [149] applied high-frequency ultrasonic loading (20 kHz) to BMG, which can be used in a few seconds well below its yield strength (~35 MPa) and well below the glass transition temperature (close to room temperature). Uniform plastic rheology is rapidly generated in the interior. The superplasticity is attributed to the dynamic heterogeneity in the BMG and the cycle-induced expansion at the atomic scale, which leads to the remarkable rejuvenation and eventual collapse of the BMG, leading to the overall fluid-like behavior. It should be noted that too large of an amplitude or too long of a sonication time will lead to the precipitation of the crystal phase and affect the performance of BMGs [146,150].

3.2 Plastic deformation

3.2.1 Non-uniform plastic deformation

Plastic deformation, such as pre-compression [66,151], is one method for rejuvenating MGs. For example, FAN et al [66] increased the ΔH_{rel} of $Cu_{48}Zr_{48}Al_4$ BMG through plastic compression, and after the plastic strain reached 10%, the ΔH_{rel} increased from 8.54 J/g in the as-cast BMG to 11.91 J/g. During pre-deformation, FV generation competes with annihilation. FV production is annihilated in equilibrium when a state of dynamic equilibrium between the two competing processes is reached. Therefore, the FV can reach a saturation state at a critical strain/stress state. DING et al [152] designed a tipping shock compression technique to achieve ultra-fast rejuvenation of the MG, which was attributed to the fact that higher stress levels can be quickly reached at high shock velocities, resulting in faster shear transformation activation and generating FV. The shock compression technology can realize the rejuvenation of MG in the nanosecond time scale, which is the shortest time-consuming among many rejuvenation methods and is accompanied by high levels of rejuvenation.

In addition to conventional pre-compression, severe plastic deformation under mechanical constraints [73], including cold rolling, wire drawing, high-pressure torsion (HPT), shot peening, mechanical milling, equal-channel angular pressing, etc., can achieve a large plastic flow and also induce rejuvenation of MGs [46,65,67,69,70, 153,154]. JOO et al [153] observed enhanced tensile ductility and work hardening behavior of HPT-BMG, with more pronounced changes in FV caused by severe plastic strain than hydrostatic pressure. The introduction of new FV with larger size by HTP creates a heterogeneous structure of BMGs at the nanoscale and leads to the multiplication of SBs. Compared with other methods to rejuvenation by plastic deformation, such as cold rolling or shot peening, HPT can induce higher strains and deform the entire sample, not just the surface. LI et al [154] achieved extreme

rejuvenation of MG by exploiting the severe plastic deformation between MG powders due to frequent shearing and collisions during mechanical milling. As shown in Fig. 10, most thermal and mechanical processing-induced energy states are lower than those induced by mechanical milling. Therefore, mechanical milling-induced rejuvenation is considered an easy and efficient method of promoting MG into a high overall energy state.

3.2.2 Uniform plastic deformation

The introduction of uniform plastic deformation is believed to promote the rejuvenation of BMG [68,155]. PAN et al [68] effectively suppressed

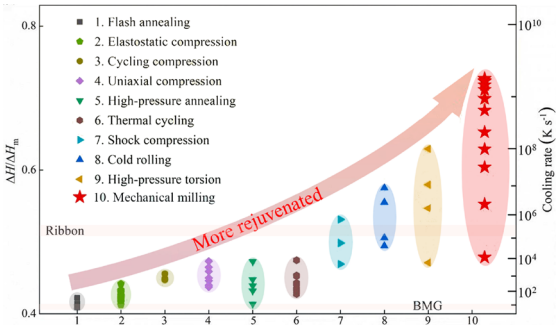

Fig. 10 Comparison among various rejuvenation methods in terms of energy [154]

shear deformation by introducing a three-dimensional stress state and achieved uniform deformation of $Zr_{64.13}Cu_{15.75}Ni_{10.12}Al_{10}$ BMG under room temperature compression by introducing a notch to the central region (see Fig. 11(a) for the process [3]). The structural change during the deformation of MGs can be viewed as competing mechanisms between shear-induced FV generation and diffusion-induced FV annihilation. Three-dimensional compressive stress inhibits atomic diffusion, and the rate of FV generation is always greater than the annihilation rate. At the same time, since the shear stress is lower than the σ_c generated by SB, strain localization is effectively avoided. Under the confinement of the three-dimensional stress, the FV of the BMG continues to increase steadily during the deformation process and finally produces a violent rejuvenation and softening [156−158]. Figure 11(b) shows the hardness contour map after 40% compression deformation; the BMG softens in a large area due to the confinement of the notch. As shown in Figs. 11(c) and (d), the ΔH_{rel} of the deformed BMG is larger than that of the as-cast BMG, and the deformation energy stored by this method is close to 30%, which

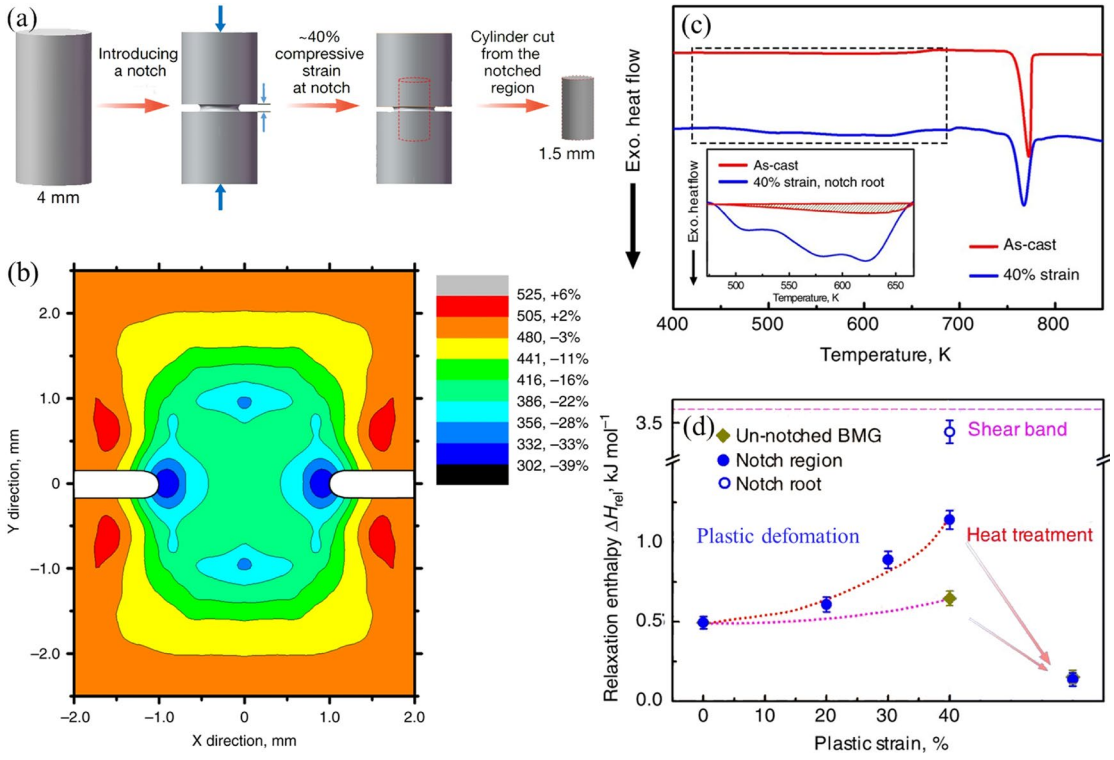

Fig. 11 (a) Process diagram leading to BMG recovery after introduction of 3D stress through circumferential notching [3]; (b) Hardness contour map with 40% strain; (c) DSC traces of as-cast and notched specimen compressed to 40% strain; (d) ΔH_{rel} of BMGs compressed to different strains and annealed heat treatment [68]

is three times that of the conventional uniaxial compression method. With or without three-dimensional stress field confinement, the ΔH_{rel} of the BMG increases with the amount of deformation, but the latter increases much more for the BMG induced by the three-dimensional stress field. MG under a 3D compressive stress field can be deformed to obtain an amorphous state equivalent to a cooling rate of up to 10^{10} K/s. This is a much higher rejuvenation effect compared to other rejuvenation methods and an order of magnitude higher than the equivalent cooling rate of the rejuvenated energy state induced by mechanical milling (see Fig. 10).

Although severe plastic deformation and uniform plastic deformation have notable effects on enhancing the energy state of MGs, the sample size of MG that can be processed via severe plastic deformation is limited. Moreover, uniform plastic deformation, such as notched compression, constitutes a destructive rejuvenation method. These disadvantages somewhat restrict their application to large-sized samples.

4 Thermomechanical coupling

4.1 Thermomechanical creep

In addition, applying a temperature below T_g during pre-elastic loading can form thermo-mechanical creep, promoting MG rejuvenation effect [45,72−75]. A reasonable temperature setting has a positive effect on rejuvenation, while a too low temperature has no noticeable effect on rejuvenation [144]. The thermomechanical creep method has the advantage of continuously tuning the MG structure by controlling temperature, stress, and time [74]. Thermomechanical creep causes structural disorder only when the applied stress exceeds a critical value. When the applied stress exceeds a critical value numerically close to the steady state flow stress, the creeping glass will return to a high enthalpy disordered state; conversely, the MG will age [159].

Applying pressure may simultaneously promote thermal regeneration [54,57,160,161] and introduce a short-range ordered (SRO) structure [160]. Figure 12 shows a schematic representation of the properties of pure thermal regeneration and pressure-promoted thermal regeneration, which summarizes the energy, density, and SRO for unquenched, pure thermally aged and rejuvenated, and pressure-promoted thermal rejuvenation. Compared with thermal rejuvenation, both the application of high pressure and the slow cooling phase after thermal annealing promoted more SRO formation, resulting in an increase in density. On the other hand, the rejuvenation effect of high pressure on the matrix is particularly significant, resulting in a high overall energy state of the MG.

It is essential to emphasize that thermo-mechanical creep does not always achieve the rejuvenation of MG; it can also push MG into a state of low energy or even exacerbate its structural relaxation. The key of promoting rejuvenation via thermomechanical creep is controlling temperature, stress, and time. However, there are still difficulties

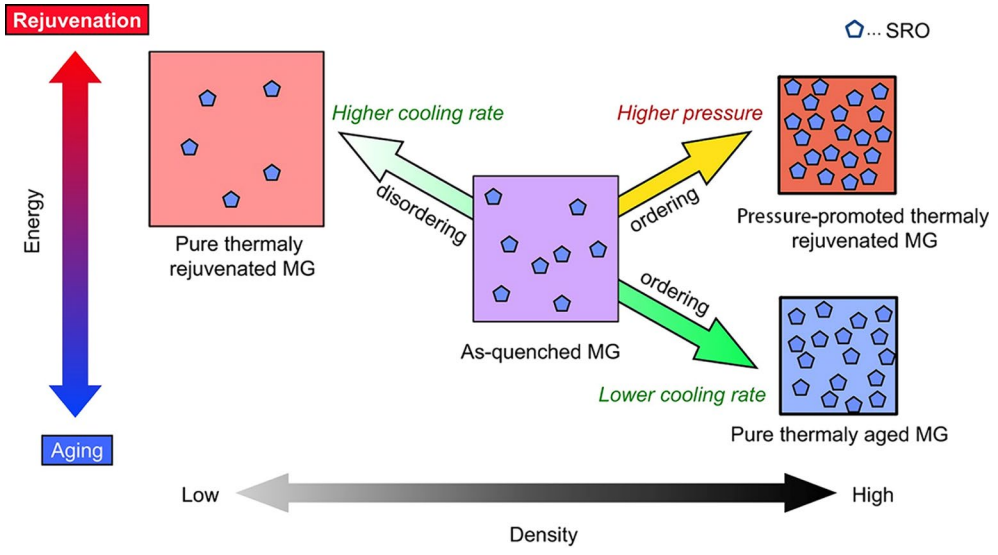

Fig. 12 Schematic illustration of rejuvenation and aging with and without pressure [160]

in precisely controlling these parameters. Moreover, the competitive behavior between rejuvenation and aging under thermomechanical creep conditions remains to be further investigated.

4.2 Thermoplastic deformation

The above plastic deformation promoting rejuvenation is carried out at room temperature, and some special thermoplastic deformation in the SLRs can also promote the rejuvenation of BMGs [76,77]. Applying a high strain rate to a supercooled liquid can excite the liquid, while cooling causes the excited liquid to freeze into a glass with a higher fictive temperature. During the thermoplastic treatment in the subcooled liquid region, the atomic structure of the MG undergoes an extensive shear rearrangement, which will cause uniform expansion of the entire sample and lead to the generation of a large number of FVs [76]. The high strain causes the MG structure to expand, which energetically pulls the structure to the high-energy region. After further cooling, the resulting excitation liquid freezes into an excitation glass. The resulting excited liquid stems from the changing competition between structural relaxation and strain recovery. The strain of the supercooled liquid counteracts the relaxation process and prevents the liquid from exhibiting its metastable equilibrium, resulting in an excited state that is in contrast to the unstrained state. The ductility is significantly improved compared to constrained materials [77]. Several BMG processing techniques can be extended to excited liquid cooling, including drawing/ extrusion, hot rolling, cold die blow molding [77], and hot-drawn [76]. High strains are introduced in the deformation zone due to geometrical changes, and the cooling rate continuously increases due to changes in cross-section or surface area.

Moreover, ZU et al [78−80] proposed a high rheological rate forming (HRRF) method to transfer mechanical work into the supercooled liquid to enhance the internal energy of BMG and significantly improve its plasticity. As shown in Fig. 13(a), BMG heated into the SLR was extruded through narrow channels at high molding pressure and finally compressed into a predetermined shape in a mold (example of molded samples in Fig. 13(b)). The BMG was extruded through the narrow channels to achieve large thermoplastic deformations and then rapidly formed at high molding pressures to reach the HRRF. Due to the atomic rearrangement inside the HRRF-treated MG, it has high plasticity, which can be achieved through the HRRF method. Since the atoms in the HRRF-treated MG are rearranged and have high internal energy storage, the sparseness of the atomic arrangement in the soft zone and hard zone in the MG is closely related to the change of potential energy. As shown in Fig. 13(c), with the increase of potential energy, the soft zone atoms are more loosely arranged (from B to D), while the hard zone is more densely arranged (from A to C). In other words, introducing high energy can effectively enhance the microscale inhomogeneity.

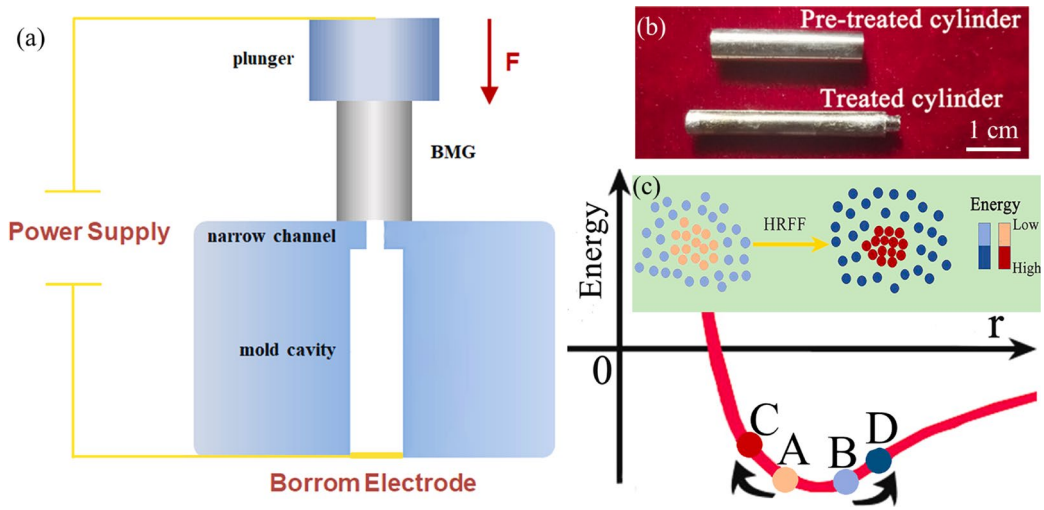

Fig. 13 (a) Schematic of HRRF method; (b) Pre-treated and treated BMG samples; (c) Schematic diagram of Lennard-Jones-like potentials (Insets are schematic illustration of the atomic arrangement structures) [80]

5 Irradiation-induced rejuvenation

In addition to the effects of force and thermal rejuvenation on MGs, irradiation also induces the rejuvenation of MGs, enhancing plasticity [30,31,82,162−169]. During irradiation, incident electrons, protons, neutrons, ions, etc, various high-energy particles and target atoms in the MG create a severe inelastic collision, resulting in target atom delocalization. These delocalized atoms continue to expand with the neighboring atoms, and the sustained displacement cascade leads to the generation of local defects and atomic rearrangement [31]. Moreover, the displacement cascades resulting from interactions disrupt the short-range ordered structure of MGs, which is believed to be the key to inducing rejuvenation [166,170,171]. HEO et al [82] found that displacement cascades due to multiple collisions disrupt the atomic configuration and reduce the initial icosahedral density by breaking local symmetry. Moreover, irradiation splits large icosahedral clusters into small ones. As shown in Fig. 14, the pair distribution function curve of the irradiated MG has a lower and broader peak compared to unirradiated MG, indicating that the neutron collision cascade promotes structural disorder in MG, i.e., irradiation induces regeneration [166]. Furthermore, annealing eliminated the irradiation-induced rejuvenation effect.

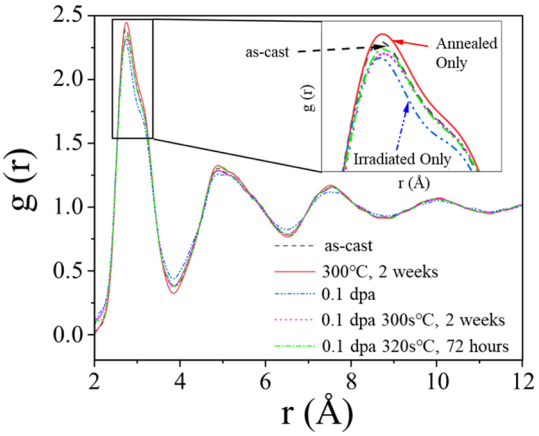

Fig. 14 Pair distribution function for neutron-irradiated and annealed $Zr_{52.5}Cu_{17.9}Ni_{14.6}Al_{10}Ti_5$ BMG [166]

Irradiation can induce MG rejuvenation, relaxation, and crystallization, depending mainly on the initial state and irradiation conditions. Remarkably, the irradiation dose significantly affects the structural evolution of MG [31,172]. Low-dose irradiation is usually favorable for inducing rejuvenation and enhancing the plasticity of MG. For example, BIAN et al [31] found that low-dose (0.5 dpa) irradiation not only promotes viscous flow and FV homogeneity in $Zr_{50.7}Cu_{28}Ni_9Al_{12.3}$ MG but also increases the FV fraction, leading to an increase in the plasticity from ~7.5% to ~11.0% after irradiation. FV annihilation occurs after the irradiation dose further increases, and structural relaxation gradually dominates, even forming nanocrystals in the MG matrix. Altogether, regulating the irradiation dose is key to promoting the rejuvenation of MG. Furthermore, it is essential to emphasize that irradiation-induced rejuvenation usually occurs only on the MG surface or in a limited size range, whereas achieving rejuvenation of BMG with a large size is difficult.

6 Free volume gradient rejuvenation

Gradient structure design has been widely used to improve material properties. FV gradients, including soft shell-hard core, hard shell-soft core, and two-dimensional distributions structures, etc, are considered effective in enhancing the plasticity of BMGs [173−176]. Gradient rejuvenation is a crucial method to prepare an FV gradient. A number of gradient rejuvenation methods have been developed, including specially designed asymmetric recovery annealing [174], modified DCT and fast cooling (FC) methods that exploit the difference in cooling rates between the center and edge of the sample [173], lateral elastostatic preloading [132], and surface mechanical attrition treatment (SMAT) [175], etc. Among them, asymmetric recovery annealing and modified DCT and FC methods belong to thermal-based approaches, while lateral elastostatic preloading and SMAT are mechanically driven.

The enhanced plasticity of BMG due to this FV gradient is attributed to the ability of the FV gradient to produce SB deflection, which can cause branching of the SB and enhance plasticity [173−175]. What is the reason for the change in SB deflection? According to the Mohr-Coulomb criterion, the effective shear stress (τ_c) and σ_c formed by the SB are calculated as follows [174]:

$$\tau_c=\tau_0-\alpha\cdot\sigma_n \quad (3)$$

$$\sigma_c=\frac{\tau_0}{\sin\theta(\cos\theta-\alpha\sin\theta)} \tag{4}$$

$$\alpha=\frac{\cos 2\theta_c}{\sin 2\theta_c} \tag{5}$$

where τ_0 is a constant, σ_n is the normal stress, θ is the SB angle between the shear surface and the loading axis, α is the normal stress coefficient, θ_c is the SB angle, and σ_c has the minimum value at this angle.

The values of local α and θ_c are determined by the FV. The local FV content controls the SB angle and the maximum effective shear stress [174]. The LLRs share in the high FV region is so large that it can suppress cavitation/fracture while promoting SB formation [175−177]. The lower the FV in the BMG, the greater the atomic friction, the greater the α, and the smaller the SB angle formed during the compressive deformation. Therefore, the SB angle at a low FV position should be smaller than that at a high FV position (Fig. 15(a)). In addition, the increased atomic friction makes initiating and propagating SBs more difficult [178]. When SB propagates at an angle of θ_c, the value of σ_c is minimized. If θ_c changes at some stage during propagation, the SB plane may form a non-uniform surface with a curved shape. The primary SB starts at low FV and propagates to high FV. Two deflections occur during the propagation, forming a curved shear surface, and further propagation is stopped. During the progression from low FV to high FV, the SB is deflected, producing a large SB angle, which indicates that θ_c is large in the region of high FV. It is noteworthy that the tangential angle between the deflection point and the two SBs forms a branch SB. However, the SB propagating from the high FV to the low FV stops without significant deflection. Therefore, it is better to stop rather than deflect and propagate the SB as it progresses from the region of high FV to low FV. Figure 15(a) shows a schematic diagram of SB propagation and branching, which stops when two different SBs start from the low FV and high FV regions and propagate in opposite directions in a BMG sample with gradient FV content. The SB is interrupted during propagation, forming a flat, complete shear plane across the BMG sample. In further plastic deformation, other new SBs are initiated in new locations. Multiple SBs intersect during propagation, which causes the shear stress at the shear surface to dissipate. As a result, the formation of a complete shear zone becomes more difficult, and hence, the fracture is delayed, which facilitates the subsequent initiation of a new shear zone, achieving plasticity enhancement (Fig. 15(b)).

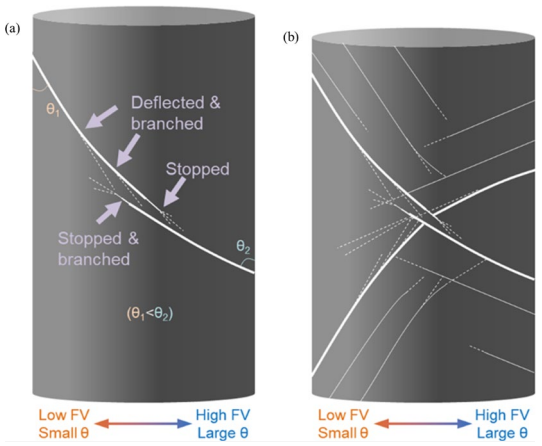

Fig. 15 (a) Schematic diagram of propagation, deflection, branching, and stopping of SBs initiated on surfaces of low FV and high FV parts; (b) Schematic diagram of initiations of new SBs without forming complete SB during deformation of heat-treated BMG sample [174]

It should be noted that only a proper FV gradient will improve the plasticity of BMG, while too high FV gradient value will lead to the sudden release of the large stress concentration in the gradient region and lead to brittle fracture, which is not conducive to the enhancement of plasticity [24,177].

7 Summary and outlook

The imperative need to improve room-temperature plasticity in MGs remains a critical challenge for their utilization as advanced structural materials. This study comprehensively consolidates a range of methodologies and mechanisms enhancing the plasticity of MGs via rejuvenation. The FV content and plasticity of low-fragility MGs can also be increased by thermal-activated, mechanical-driven, thermo-mechanically coupled, and irradiation-inducing rejuvenation. The rejuvenation treatments can increase the free volume content within the MGs, enhance structural heterogeneity and promote SB formation. Moreover, gradient rejuvenation can promote the gradient distribution of FV, leading to SB deflection and

plasticity enhancement.

Although great progress has been made in exploring and enhancing the plasticity of MGs, and these–methods can be learned or applied in most MG systems, more work is still to be expected, as follows.

(1) At present, MGs can have extensive compressive plasticity after DCT, but tensile plasticity has not been found so far. The microstructure that can effectively relax the stress concentration and inhibit the rapid expansion of SB may be expected to significantly improve the plastic deformation ability of MGs and even produce tensile plasticity and work hardening effects.

(2) Although DCT, the introduction of 3D stress state and deformation can effectively promote rejuvenation, these methods have many shortcomings, such as the limited size of DCT rejuvenation specimens, and notching could destroy the integrity of the MG. Pure thermal rejuvenation may be the most meaningful means of rejuvenation, but the work reported so far is mostly single pass pure thermal annealing + quenching, and whether multiple cycles of pure thermal annealing + quenching can achieve a higher level of MG rejuvenation will be worth further studying.

(3) What factors determine the upper limit of rejuvenation for MGs? Can tensile plasticity in MGs be achieved through continuous rejuvenation?

(4) What effect does the coupling of multiple rejuvenation methods produce? Can plasticity be further improved?

CRediT authorship contribution statement

Quan DONG: Writing – Original draft, Writing – Review & editing; **Cai-ju LI:** Writing – Review & editing, Supervision; **Baran SARAC:** Writing – Review & editing; **Jürgen ECKERT:** Conceptualization, Writing – Original draft, Writing – Review & editing, Supervision; **Jun TAN:** Conceptualization, Writing – Original draft, Writing – Review & editing, Supervision.

Declaration of competing interest

The authors declare that they have no known competing financial interests or personal relationships that could have appeared to influence the work reported in this paper.

Acknowledgments

We thank W. H. WANG, Y. H. LIU, and B. A. SUN of the Institute of Physics, Chinese Academy of Sciences, G. WANG of the Shanghai University, and Z. F. ZHANG of the Institute of Metal Research, Chinese Academy of Sciences for fruitful discussions and valuable comments. The authors acknowledge the funding support from the National Natural Science Foundation of China (Nos. 51301078, 51361017, 51461026, 51861016, 52061021), the European Research Council (Nos. ERC-2013-ADG-340025, ERC-2019-PoC-862485), and the Austrian Science Fund (No. I3937-N36).

References

[1] LI H X, LU Z C, WANG S L, WU Y, LU Z P. Fe-based bulk metallic glasses: Glass formation, fabrication, properties and applications [J]. Progress in Materials Science, 2019, 103: 235−318.

[2] LI C J, TAN J, WANG G, BEDNARČÍK J, ZHU X K, ZHANG Y, STOICA M, KÜHN U, ECKERT J. Enhanced strength and transformation-induced plasticity in rapidly solidified Zr−Co−(Al) alloys [J]. Scripta Materialia, 2013, 68: 897−900.

[3] PAN J, IVANOV Y P, ZHOU W H, LI Y, GREER A L. Strain-hardening and suppression of shear-banding in rejuvenated bulk metallic glass [J]. Nature, 2020, 578: 559−562.

[4] ZHANG Jia-jia, LIU Wen-sheng, MA Yun-zhu, YE Xiao-shan, WU Ya-yu, HUANG Bo-yun. Preparation and properties of $Ni_{68.6}W_{17.9}B_{13.5}$ metallic glass [J]. Transactions of Nonferrous Metals Society of China, 2015, 25: 1575−1579.

[5] HUANG Yong-jiang, SHEN Jun, SUN Yi, SUN Jian-fei. Indentation size effect of hardness of metallic glasses [J]. Materials & Design, 2010, 31: 1563−1566.

[6] ZHANG Mao, MA Yun-fei, HUANG Ting, GONG Pan, WANG Ying, CAI Hong-jun, LI Qiao-min, WANG Xin-yun, DENG Lei. High-temperature oxidation behavior of $Cu_{64}Zr_{36}$ metallic glass powders [J]. Transactions of Nonferrous Metals Society of China, 2023, 33: 1814−1826.

[7] WU J, ZHANG S D, SUN W H, GAO Y, WANG J Q. Enhanced corrosion resistance in Fe-based amorphous coatings through eliminating Cr-depleted zones [J]. Corrosion Science, 2018, 136: 161−173.

[8] NAYAK S K, KUMAR A, LAHA T. Fe-based metallic glass coatings by thermal spraying: A focused review on corrosion properties and related degradation mechanisms [J]. International Materials Reviews, 2023, 68: 404−485.

[9] ZHANG Ting, LONG Zhi-lin, PENG Li. Glass forming ability prediction of bulk metallic glasses based on fused strategy [J]. Transactions of Nonferrous Metals Society of China, 2024, 34: 1558−1570.

[10] ZUO Ting-ting, GAO M C, OUYANG Li-zhi, YANG Xiao, CHENG Yong-qiang, FENG Rui, CHEN Shu-ying, LIAW P K, HAWK J A, ZHANG Yong. Tailoring magnetic behavior of CoFeMnNiX (X= Al, Cr, Ga, and Sn) high entropy alloys by metal doping [J]. Acta Materialia, 2017, 130: 10−18.

[11] LIU W J, ZHANG H X, SHI J A, WANG Z C, SONG C,

WANG X R, LU S Y, ZHOU X J, GU L, LOUZGUINE-LUZGIN D V, CHEN M W, YAO K F, CHEN N. A room-temperature magnetic semiconductor from a ferromagnetic metallic glass [J]. Nature Communications, 2016, 7: 13497.

[12] LI X S, ZHOU J, SHEN L Q, SUN B A, BAI H Y, WANG W H. Exceptionally high saturation magnetic flux density and ultralow coercivity via an amorphous-nanocrystalline transitional microstructure in an FeCo-based alloy [J]. Advanced Materials, 2023, 35: 2205863.

[13] JIA Zhe, NOMOTO K, WANG Qing, KONG C, SUN Li-gang, ZHANG Lai-chang, LIANG Shun-xing, LU Jian, KRUZIC J J. A self-supported high-entropy metallic glass with a nanosponge architecture for efficient hydrogen evolution under alkaline and acidic conditions [J]. Advanced Functional Materials, 2021, 31: 2101586.

[14] LIU Si-da, LI Hong-kun, ZHONG Jing, XU Kai, WU Ge, LIU Chang, ZHOU Bin-bin, YAN Yang, LI Lan-xi, CHA Wen-hao, CHANG Ke-ke, LI Yang-yang, LU Jian. A crystal glass-nanostructured Al-based electrocatalyst for hydrogen evolution reaction [J]. Science Advances, 2022, 8: eadd6421.

[15] GAO Fei-yue, LIU Si-nan, GE Jia-cheng, ZHANG Xiao-long, ZHU Li, ZHENG Ya-rong, DUAN Yu, QIN Shuai, DONG Wei-xia, YU Xing-xing, BAO Rui-cheng, YANG Peng-peng, NIU Zhuang-zhuang, DING Zhi-gang, LIU Wei, LAN Si, GAO Min-rui, YAN Yu-shan, YU Shu-hong, Nickel–molybdenum–niobium metallic glass for efficient hydrogen oxidation in hydroxide exchange membrane fuel cells [J]. Nature Catalysis, 2022, 5: 993−1005.

[16] BIN S J B, FONG K S, CHUA B W, GUPTA M. Mg-based bulk metallic glasses: A review of recent developments [J]. Journal of Magnesium and Alloys, 2022, 10: 899−914.

[17] DING Da-wei, TAN Jing, CAI An-hui, LIU Yong, WU Hong, AN Qi, LI Peng-wei, ZHANG Yan, YANG Qing. Fe−C micro-alloying effect on properties of $Zr_{53}Al_{11.6}Ni_{11.7}Cu_{23.7}$ bulk metallic glass [J]. Transactions of Nonferrous Metals Society of China, 2021, 31: 2750−2761.

[18] XU Hong-wei, DU Yu-lei, DENG Yu. Effect of minor-addition of Fe on structural and mechanical properties of CuZrAl bulk metallic glass [J]. Transactions of Nonferrous Metals Society of China, 2012, 22: 1123−1126.

[19] DONG Q, PAN Y J, TAN J, QIN X M, LI C J, GAO P, FENG Z X, CALIN M, ECKERT J. A comparative study of glass-forming ability, crystallization kinetics and mechanical properties of $Zr_{55}Co_{25}Al_{20}$ and $Zr_{52}Co_{25}Al_{23}$ bulk metallic glasses [J]. Journal of Alloys and Compounds, 2019, 785: 422−428.

[20] WANG D P, ZHAO D Q, DING D W, BAI H Y, WANG W H. Understanding the correlations between Poisson's ratio and plasticity based on microscopic flow units in metallic glasses [J]. Journal of Applied Physics, 2014, 115: 123507.

[21] LIU Y H, WANG G, WANG R J, ZHAO D Q, PAN M X, WANG W H. Super plastic bulk metallic glasses at room temperature [J]. Science, 2007, 315: 1385−1388.

[22] KIM S Y, OH H S, PARK E S. A hidden variable in shear transformation zone volume versus Poisson's ratio relation in metallic glasses [J]. APL Materials, 2017, 5: 106105.

[23] HUA Neng-bin, CHEN Wen-zhe. Enhancement of glass-forming ability and mechanical property of Zr-based Zr−Al−Ni bulk metallic glasses with addition of Pd [J]. Journal of Alloys and Compounds, 2017, 693: 816−824.

[24] LI T H, LIAO Y C, SONG S M, JIANG Y L, TSAI P H, JANG J S C, HUANG J C. Significantly enhanced mechanical properties of ZrAlCo bulk amorphous alloy by microalloying with Ta [J]. Intermetallics, 2018, 93: 162−168.

[25] LUO Y S, WANG Z, QIAO J W. Flow serrations of rejuvenation behaviour through cryogenic thermal cycling for Zr-based bulk metallic glass [J]. Philosophical Magazine, 2021, 101: 2261−2272.

[26] KETOV S V, SUN Y H, NACHUM S, LU Z, CHECCHI A, BERALDIN A R, BAI H Y, WANG W H, LOUZGUINE-LUZGIN D V, CARPENTER M A, GREER A L. Rejuvenation of metallic glasses by non-affine thermal strain [J]. Nature, 2015, 524: 200−203.

[27] DI Si-yi, WANG Qian-qian, YANG Yi-yuan, LIANG Tao, ZHOU Jing, SU Lin, YIN Kui-bo, ZENG Qiao-shi, SUN Li-tao, SHEN Bao-long. Efficient rejuvenation of heterogeneous $\{[(Fe_{0.5}Co_{0.5})_{0.75}B_{0.2}Si_{0.05}]_{96}Nb_4\}_{99.9}Cu_{0.1}$ bulk metallic glass upon cryogenic cycling treatment [J]. Journal of Materials Science & Technology, 2022, 97: 20−28.

[28] ZHU Yu-hui, ZHOU Yong-kang, WANG Ai-min, LI Hong, FU Hua-meng, ZHANG Hong-wei, ZHANG Hai-feng, ZHU Zheng-wang. Atomic-scale icosahedral short-range ordering in a rejuvenated Zr-based bulk metallic glass upon deep cryogenic treatment [J]. Materials Science and Engineering A, 2022, 850: 143565.

[29] GUO Wei, SHAO Yu-man, ZHAO Mi, LÜ Shu-lin, WU Shu-sen. Varying the treating conditions to rejuvenate metallic glass by deep cryogenic cycling treatment [J]. Journal of Alloys and Compounds, 2020, 819: 152997.

[30] SUN K, WANG G, WANG Y W, CHEN H C, YAN L, PAULY S, WU Y H, WEBER H, WANG Q, HUANG B, JIA Y D, YI J, ZHAI Q J. Structural rejuvenation and relaxation of a metallic glass induced by ion irradiation [J]. Scripta Materialia, 2020, 180: 34−39.

[31] BIAN X L, WANG G, CHEN H C, YAN L, WANG J G, WANG Q, HU P F, REN J L, CHAN K C, ZHENG N, TERESIAK A, GAO Y L, ZHAI Q J, ECKERT J, BEADSWORTH J, DAHMEN K A, LIAW P K. Manipulation of free volumes in a metallic glass through Xe-ion irradiation [J]. Acta Materialia, 2016, 106: 66−77.

[32] HILKE S, RÖSNER H, WILDE G. The role of minor alloying in the plasticity of bulk metallic glasses [J]. Scripta Materialia, 2020, 188: 50−53.

[33] STOICA M, VAN STEENBERGE N, BEDNARČIK J, MATTERN N, FRANZ H, ECKERT J. Changes in short-range order of $Zr_{55}Cu_{30}Al_{10}Ni_5$ and $Zr_{55}Cu_{20}Al_{10}Ni_{10}Ti_5$ BMGs upon annealing [J]. Journal of Alloys and Compounds, 2010, 506: 85−87.

[34] ZHOU Wei, HU Jia-qi, WENG Wen-ping, GAO Ling-yan, XU Guang-ying. Enhancement of plasticity in Zr−Cu−Ni−Al−Ti bulk metallic glass by heterogeneous microstructure [J]. Journal of Non-Crystalline Solids, 2018, 481: 530−536.

[35] WU F F, JIANG S S, ZHAO R D, ZHOU Q, ZHANG G A, WU X F. Size-dependent plastic stability of Zr-based metallic glass [J]. Materials Science and Engineering: A, 2015, 646: 272−278.

[36] ZHANG Shan, WEI Chao, YANG Liang, LV Jing-wang, SHI Zhi-lin, ZHANG Hao-ran, ZHANG Xin-yu, MA Ming-zhen. Effects of sample diameter, aspect ratio, and strain rate on compressive deformation and fracture behavior of $Zr_{50}Cu_{34}Al_8Ag_8$ metallic glass [J]. Journal of Non-Crystalline Solids, 2022, 587: 121583.

[37] CHEN S H, CHAN K C, XIA L. Deformation behavior of a Zr-based bulk metallic glass under a complex stress state [J]. Intermetallics, 2013, 43: 38−44.

[38] CHEN S H, CHAN K C, XIA L. Effect of stress gradient on the deformation behavior of a bulk metallic glass under uniaxial tension [J]. Materials Science and Engineering: A, 2013, 574: 262−265.

[39] ZHAO Lei, HAN Dong-xue, GUAN Shuai, LU Xian-zheng, CHAN Kang-cheung, WANG Gang. Simultaneous improvement of plasticity and strength of metallic glasses by tailoring residual stress: Role of stress gradient on shear banding [J]. Materials & Design, 2021, 197: 109246.

[40] QU R T, ZHAO J X, STOICA M, ECKERT J, ZHANG Z F. Macroscopic tensile plasticity of bulk metallic glass through designed artificial defects [J]. Materials Science and Engineering: A, 2012, 534: 365−373.

[41] ZHAI Hai-min, WANG Hai-feng, LIU Feng. Effect of minor Nb addition on mechanical properties of in-situ Cu-based bulk metallic glass composite [J]. Transactions of Nonferrous Metals Society of China, 2017, 27: 363−368.

[42] DONG Quan, TAN Jun, LI Cai-ju, SARAC B, ECKERT J. Room-temperature plasticity of metallic glass composites: A review [J]. Composites Part B: Engineering, 2024, 280: 111453.

[43] PARISI G, SCIORTINO F. Flying to the bottom [J]. Nature Materials, 2013, 12: 94−95.

[44] SAIDA J, YAMADA R, WAKEDA M, OGATA S. Thermal rejuvenation in metallic glasses [J]. Science and Technology of Advanced Materials, 2017, 18: 152−162.

[45] TONG Y, IWASHITA T, DMOWSKI W, BEI H, YOKOYAMA Y, EGAMI T. Structural rejuvenation in bulk metallic glasses [J]. Acta Materialia, 2015, 86: 240−246.

[46] MENG F, TSUCHIYA K, KRAMER M J, OTT R T. Reduction of shear localization through structural rejuvenation in Zr−Cu−Al bulk metallic glass [J]. Materials Science and Engineering: A, 2019, 765: 138304.

[47] TAO K, LI F C, LIU Y H, PINEDA E, SONG K K, QIAO J C. Unraveling the microstructural heterogeneity and plasticity of $Zr_{50}Cu_{40}Al_{10}$ bulk metallic glass by nanoindentation [J]. International Journal of Plasticity, 2022, 154: 103305.

[48] SONG Wen-li, MENG Xiao-he, WU Yuan, CAO Di, WANG Hui, LIU Xiong-jun, WANG Xian-zhen, LU Zhao-ping. Improving plasticity of the $Zr_{46}Cu_{46}Al_8$ bulk metallic glass via thermal rejuvenation [J]. Science Bulletin, 2018, 63: 840−844.

[49] GUO Wei, SHAO Yu-man, SAIDA Jun-ji, ZHAO Mi, LÜ Shu-lin, WU Shu-sen. Rejuvenation and plasticization of Zr-based bulk metallic glass with various Ta content upon deep cryogenic cycling [J]. Journal of Alloys and Compounds, 2019, 795: 314−318.

[50] GUO Wei, SAIDA Jun-ji, ZHAO Mi, LÜ Shu-lin, WU Shu-sen. Rejuvenation of Zr-based bulk metallic glass matrix composite upon deep cryogenic cycling [J]. Materials Letters, 2019, 247: 135−138.

[51] PENG Zhen, CHEN Yu-mei, YIN Geng, GONG Pan, JAMILI-SHIRVAN Z, LI Ning, WANG Xin-yun, YAO Ke-fu. Effect of cryogenic cycling on mechanical properties of ZrTiCuNiBe bulk metallic glass [J]. Fundamental Research, 2022, 2: 764−775.

[52] GREER A L, SUN Y H. Stored energy in metallic glasses due to strains within the elastic limit [J]. Philosophical Magazine, 2016, 96: 1643−1663.

[53] KETOV S V, TRIFONOV A S, IVANOV Y P, CHURYUMOV A Y, LUBENCHENKO A V, BATRAKOV A A, JIANG J, LOUZGUINE-LUZGIN D V, ECKERT J, ORAVA J, GREER A L. On cryothermal cycling as a method for inducing structural changes in metallic glasses [J]. NPG Asia Materials, 2018, 10: 137−145.

[54] LI Hong, JIN Cheng-gang, SHA Zhen-dong. The effect of pressure-promoted thermal rejuvenation on the fracture energy of metallic glasses [J]. Journal of Non-Crystalline Solids, 2022, 590: 121674.

[55] KÜCHEMANN S, DERLET P M, LIU C Y, ROSENTHAL D, SPARKS G, LARSON W S, MAAß R. Energy storage in metallic glasses via flash annealing [J]. Advanced Functional Materials, 2018, 28: 1805385.

[56] WAKEDA M, SAIDA J, LI J, OGATA S. Controlled rejuvenation of amorphous metals with thermal processing [J]. Scientific Reports, 2015, 5: 10545.

[57] LI S, ZHANG J C, SHA Z D. Mechanical behavior of metallic glasses with pressure-promoted thermal rejuvenation [J]. Journal of Alloys and Compounds, 2020, 848: 156597.

[58] ZHANG S Y, ZHOU W H, SONG L J, HUO J T, YAO J H, WANG J Q, LI Y. Decoupling between enthalpy and mechanical properties in rejuvenated metallic glass [J]. Scripta Materialia, 2023, 223: 115056.

[59] SAMAVATIAN M, GHOLAMIPOUR R, AMADEH A A, MIRDAMADI S. Role of tensile elastostatic loading on atomic structure and mechanical properties of $Zr_{55}Cu_{30}Ni_5Al_{10}$ bulk metallic glass [J]. Materials Science and Engineering A, 2019, 753: 218−223.

[60] PARK K W, LEE C M, KIM H J, LEE J H, LEE J C. A methodology of enhancing the plasticity of amorphous alloys: Elastostatic compression at room temperature [J]. Materials Science and Engineering: A, 2009, 499: 529−533.

[61] PARK K W, LEE C M, WAKEDA M, SHIBUTANI Y, FALK M L, LEE J C. Elastostatically induced structural disordering in amorphous alloys [J]. Acta Materialia, 2008, 56: 5440−5450.

[62] YU P, CHAN K C, CHEN W, XIA L. Elastic moduli and mechanical properties of bulk metallic glasses after quasi-static compression [J]. Journal of Alloys and Compounds, 2011, 509: 8518−8521.

[63] SARAC B, GAMMER C, DENG L, PARK E, YOKOYAMA Y, STOICA M, ECKERT J. Elastostatic reversibility in thermally formed bulk metallic glasses: Nanobeam diffraction fluctuation electron microscopy [J]. Nanoscale, 2018, 10: 1081−1089.

[64] SOHRABI S, SUN B Y, MAHMOODAN M, SUN Y H, GHOLAMIPOUR R, WANG W H. Rejuvenation by compressive elasto-static loading: The role of static stress on a Zr-based metallic glass [J]. Journal of Alloys and Compounds, 2023, 933: 167715.

[65] HARUYAMA O, KISARA K, YAMASHITA A, KOGURE K, YOKOYAMA Y, SUGIYAMA K. Characterization of free volume in cold-rolled $Zr_{55}Cu_{30}Ni_5Al_{10}$ bulk metallic glasses [J]. Acta Materialia, 2013, 61: 3224−3232.

[66] FAN Hong-bo, WANG Nan, HE Chao, HUANG Yong-jiang, NING Zhi-liang, SUN Jian-fei. Effect of pre-straining on the structure and nano-mechanical properties of a CuZrAl bulk metallic glass [J]. Journal of Alloys and Compounds, 2022, 918: 165635.

[67] XIE Sheng-hui, KRUZIC J J. Cold rolling improves the fracture toughness of a Zr-based bulk metallic glass [J]. Journal of Alloys and Compounds, 2017, 694: 1109−1120.

[68] PAN J, WANG Y X, GUO Q, ZHANG D, GREER A L, LI Y. Extreme rejuvenation and softening in a bulk metallic glass [J]. Nature Communications, 2018, 9: 560.

[69] EBNER C, PAULY S, ECKERT J, RENTENBERGER C. Effect of mechanically induced structural rejuvenation on the deformation behaviour of CuZr based bulk metallic glass [J]. Materials Science and Engineering: A, 2020, 773: 138848.

[70] ZHOU Hong-bo, HUBEK R, PETERLECHNER M, WILDE G. Two-stage rejuvenation and the correlation between rejuvenation behavior and the boson heat capacity peak of a bulk metallic glass [J]. Acta Materialia, 2019, 179: 308−316.

[71] QIANG Jian, TSUCHIYA K. Composition dependence of mechanically-induced structural rejuvenation in Zr−Cu−Al−Ni metallic glasses [J]. Journal of Alloys and Compounds, 2017, 712: 250−255.

[72] TONG Y, DMOWSKI W, YOKOYAMA Y, WANG G, LIAW P K, EGAMI T. Recovering compressive plasticity of bulk metallic glasses by high-temperature creep [J]. Scripta Materialia, 2013, 69: 570−573.

[73] SUN Yong-hao, CONCUSTELL A, GREER A L. Thermomechanical processing of metallic glasses: extending the range of the glassy state [J]. Nature Reviews Materials, 2016, 1: 16039.

[74] TONG Y, DMOWSKI W, BEI H, YOKOYAMA Y, EGAMI T. Mechanical rejuvenation in bulk metallic glass induced by thermo-mechanical creep [J]. Acta Materialia, 2018, 148: 384−390.

[75] WANG Hao, ZHAO Cheng-liang, CHANG Chun-tao, ZHU Sheng-li, ZHAO Zhan-kui. Stress-annealing induced quasistatic creep recovery in ZrCuAlNi metallic glass [J]. Journal of Non-Crystalline Solids, 2024, 624: 122704.

[76] DONG Jie, FENG Yi-hui, HUAN Yong, YI Jun, WANG Wei-hua, BAI Hai-yang, SUN Bao-an. Rejuvenation in hot-drawn micrometer metallic glassy wires [J]. Chinese Physics Letters, 2020, 37: 017103.

[77] MOTA R M O, LUND E T, SOHN S, BROWNE D J, HOFMANN D C, CURTAROLO S, van de WALLE A, SCHROERS J. Enhancing ductility in bulk metallic glasses by straining during cooling [J]. Communications Materials, 2021, 2: 23.

[78] ZHANG Qi-dong, WANG Li-fang, ZHAO Yong, JIANG Yan, ZU Fang-qiu. Remarkable improving plasticity of a brittle Zr-based bulk metallic glass by a high rheological rate forming method in centesimal seconds [J]. Materials Letters, 2016, 164: 348−352.

[79] MA Yu-bai, WANG Bao-zhen, ZHANG Qi-dong, JIANG Yan, HOU De-wen, CUI Xiao, ZU Fang-qiu. Change dynamic behaviors by heightening its stored energy of monolithic bulk metallic glass [J]. Materials & Design, 2019, 181: 107971.

[80] MA Yu-bai, JIANG Yan, DING Hua-ping, ZHANG Qi-dong, LI Xiao-yun, ZU Fang-qiu. Torsional behaviors in Zr-based bulk metallic glass with high stored energy structure [J]. Materials Science and Engineering: A, 2019, 751: 128−132.

[81] XIAO Qiran, HUANG Li-ping, SHI Yun-feng. Suppression of shear banding in amorphous ZrCuAl nanopillars by irradiation [J]. Journal of Applied Physics, 2013, 113: 083514.

[82] HEO J, KIM S, RYU S, JANG D. Delocalized plastic flow in proton-irradiated monolithic metallic glasses [J]. Scientific Reports, 2016, 6: 23244.

[83] GUO W, YU S, DING J, LÜ S L, WU S S, ZHAO M. Tailoring rejuvenation behavior of Zr-based metallic glass upon deep cryogenic cycling treatment [J]. Transactions of Nonferrous Metals Society of China, 2024, 34: 582−591.

[84] WANG Ming-zi, GUO Wei, LÜ Shu-lin, WU Shu-sen. Effect of deep cryogenic cycling treatment on structure and properties of metallic glass: A review [J]. Transactions of Nonferrous Metals Society of China, 2023, 33: 2879−2897.

[85] GUO Wei, YAMADA Rui, SAIDA Jun-ji. Rejuvenation and plasticization of metallic glass by deep cryogenic cycling treatment [J]. Intermetallics, 2018, 93: 141−147.

[86] ZHU Qian-yong, ZHANG Min, JIN Xi, YANG Hui-jun, JIA Lan, QIAO Jun-wei. Effect of deep cryogenic cycling treatment on shear transformation zone volume and size of Zr-based metallic glass [J]. Journal of Materials Research, 2021, 36: 2047−2055.

[87] GONG Pan, YIN Geng, JAMILI-SHIRVAN Z, DING Hong-yu, WANG Xin-yun, JIN Jun-song. Influence of deep cryogenic cycling on the rejuvenation and plasticization of TiZrHfBeCu high-entropy bulk metallic glass [J]. Materials Science and Engineering: A, 2020, 797: 140078.

[88] GU Jia-lun, LUAN Heng-wei, ZHAO Shao-fan, BU Heng-tong, SI Jia-jia, SHAO yang, YAO Ke-fu. Unique energy-storage behavior related to structural heterogeneity in high-entropy metallic glass [J]. Materials Science and Engineering: A, 2020, 786: 139417.

[89] SAMAVATIAN M, GHOLAMIPOUR R, AMADEH A A, MIRDAMADI S. Correlation between plasticity and atomic structure evolution of a rejuvenated bulk metallic glass [J]. Metallurgical and Materials Transactions A, 2019, 50: 4743−4749.

[90] TANG Chun-guang, PENG Hai-long, CHEN Yu, FERRY M. Formation and dilatation of shear bands in a Cu−Zr metallic glass: A free volume perspective [J]. Journal of Applied Physics, 2016, 120: 235101.

[91] HUO L S, ZENG J F, WANG W H, LIU C T, YANG Y. The dependence of shear modulus on dynamic relaxation and evolution of local structural heterogeneity in a metallic glass

[J]. Acta Materialia, 2013, 61: 4329−4338.

[92] HUFNAGEL T C. Metallic glasses: Cryogenic rejuvenation [J]. Nature Materials, 2015, 14: 867−868.

[93] BIAN X L, WANG G, YI J, JIA Y D, BEDNARČÍK J, ZHAI Q J, KABAN I, SARAC B, MÜHLBACHER M, SPIECKERMANN F, KECKES J, ECKERT J. Atomic origin for rejuvenation of a Zr-based metallic glass at cryogenic temperature [J]. Journal of Alloys and Compounds, 2017, 718: 254−259.

[94] NAN Ce-wen. Physics of inhomogeneous inorganic materials [J]. Progress in Materials Science, 1993, 37: 1−116.

[95] LIU Z Q, LIU G, QU R T, ZHANG Z F, WU S J, ZHANG T. Microstructural percolation assisted breakthrough of trade-off between strength and ductility in CuZr-based metallic glass composites [J]. Scientific Reports, 2014, 4: 4167.

[96] DING J, INOUE A, ZHU S L, WU S L, SHALAAN E, AL-GHAMDI A A. Formation, microstructure and mechanical properties of ductile Zr-rich Zr−Cu−Al bulk metallic glass composites [J]. Journal of Materials Research and Technology, 2021, 15: 5452−5465.

[97] LIU Zeng-qian, LI Ran, LIU Gang, SU Wen-huang, WANG Hui, LI Yan, SHI Min-jie, LUO Xue-kun, WU Guo-juan, ZHANG Tao. Microstructural tailoring and improvement of mechanical properties in CuZr-based bulk metallic glass composites [J]. Acta Materialia, 2012, 60: 3128−3139.

[98] SHANG Bao-shuang, WANG Wei-hua, GREER A L, GUAN Peng-fei. Atomistic modelling of thermal-cycling rejuvenation in metallic glasses [J]. Acta Materialia, 2021, 213: 116952.

[99] KANG S J, CAO Q P, LIU J, TANG Y, WANG X D, ZHANG D X, AHN I S, CARON A, JIANG J Z. Intermediate structural state for maximizing the rejuvenation effect in metallic glass via thermo-cycling treatment [J]. Journal of Alloys and Compounds, 2019, 795: 493−500.

[100] PAN D, INOUE A, SAKURAI T, CHEN M W. Experimental characterization of shear transformation zones for plastic flow of bulk metallic glasses [J]. Proceedings of the National Academy of Sciences of the United States of America, 2008, 105: 14769−14772.

[101] ZHAI Hai-min, DU Yin, LI Xu-qiang, LI Wen-sheng, WANG Hai-feng. Improving the wear performance of a commercial Vit 1 amorphous alloy by a cryogenic cycling treatment [J]. Journal of Materials Science, 2021, 56: 8276−8287.

[102] WANG Tuo, HU Li-na, LIU Yan-hui, HUI Xi-dong. Intrinsic correlation of the plasticity with liquid behavior of bulk metallic glass forming alloys [J]. Materials Science and Engineering A, 2019, 744: 316−323.

[103] GUO Wei, SAIDA J, ZHAO Mi, LÜ Shu-lin, WU Shu-sen. Unconspicuous rejuvenation of a Pd-based metallic glass upon deep cryogenic cycling treatment [J]. Materials Science and Engineering: A, 2019, 759: 59−64.

[104] INOUE A, NEGISHI T, KIMURA H M, ZHANG T, YAVARI A R. High packing density of Zr- and Pd-based bulk amorphous alloys [J]. Materials Transactions, JIM, 1998, 39: 318−321.

[105] COSTA M B, LONDOÑO J J, BLATTER A, HARIHARAN A, GEBERT A, CARPENTER M A, GREER A L. Anelastic-like nature of the rejuvenation of metallic glasses by cryogenic thermal cycling [J]. Acta Materialia, 2023, 244: 118551.

[106] KIM Y H, LIM K R, LEE D W, CHOI Y S, NA Y S. Quenching temperature and cooling rate effects on thermal rejuvenation of metallic glasses [J]. Metals and Materials International, 2021, 27: 5108−5113.

[107] SARAC B, ZHANG L, KOSIBA K, PAULY S, STOICA M, ECKERT J. Towards the better: Intrinsic property amelioration in bulk metallic glasses [J]. Scientific Reports, 2016, 6: 27271.

[108] GUO Wei, YAMADA Rui, SAIDA Jun-ji, LÜ Shu-lin, WU Shu-sen. Thermal rejuvenation of a heterogeneous metallic glass [J]. Journal of Non-Crystalline Solids, 2018, 498: 8−13.

[109] GUO Wei, SAIDA Jun-ji, ZHAO Mi, LÜ Shu-lin, WU Shu-sen. Thermal rejuvenation of an Mg-based metallic glass [J]. Metallurgical and Materials Transactions A, 2019, 50: 1125−1129.

[110] WAKEDA M, SAIDA J. Heterogeneous structural changes correlated to local atomic order in thermal rejuvenation process of Cu−Zr metallic glass [J]. Science and Technology of Advanced Materials, 2019, 20: 632−642.

[111] HUANG Yong-jiang, FAN Hong-bo, GUAN Shi-song, NING Zhi-liang, CAO Fu-yang, DAISENBERG D, SUN Jian-fei. Fine tuning the microstructure and mechanical properties of a Zr-based bulk metallic glass using electropulsing treatment [J]. Journal of Alloys and Compounds, 2019, 789: 704−711.

[112] GONG X Y, WANG X D, ZHANG P, CAO X Z, CAO Q P, ZHANG D X, JIANG J Z. Structural rejuvenation in a Zr-based bulk metallic glass via electropulsing treatment [J]. Applied Physics Letters, 2021, 119: 043901.

[113] OKULOV I V, SOLDATOV I V, SARMANOVA M F, KABAN I, GEMMING T, EDSTRÖM K, ECKERT J. Flash Joule heating for ductilization of metallic glasses [J]. Nature Communications, 2015, 6: 7932.

[114] YIU P, JANG J S C, CHANG S Y, CHEN Y C, CHU J P, HSUEH C H. Plasticity enhancement of Zr-based bulk metallic glasses by direct current electropulsing [J]. Journal of Alloys and Compounds, 2012, 525: 68−72.

[115] JOHNSON W L, KALTENBOECK G, DEMETRIOU M D, SCHRAMM J P, LIU X, SAMWER K, KIM C P, HOFMANN D C. Beating crystallization in glass-forming metals by millisecond heating and processing [J]. Science, 2011, 332: 828−833.

[116] LIU Xiao, DEMETRIOU M D, KALTENBOECK G, SCHRAMM J P, GARRETT G R, JOHNSON W L. Description of millisecond Ohmic heating and forming of metallic glasses [J]. Acta Materialia, 2013, 61: 3060−3067.

[117] KÜCHEMANN S, SAMWER K. Ultrafast heating of metallic glasses reveals disordering of the amorphous structure [J]. Acta Materialia, 2016, 104: 119−124.

[118] KOSIBA K, PAULY S. Inductive flash-annealing of bulk metallic glasses [J]. Scientific Reports, 2017, 7: 2151.

[119] KOSIBA K, SCUDINO S, KOBOLD R, KÜHN U, GREER A L, ECKERT J, PAULY S. Transient nucleation and

microstructural design in flash-annealed bulk metallic glasses [J]. Acta Materialia, 2017, 127: 416−425.

[120] KOSIBA K, ŞOPU D, SCUDINO S, ZHANG L, BEDNARCIK J, PAULY S. Modulating heterogeneity and plasticity in bulk metallic glasses: Role of interfaces on shear banding [J]. International Journal of Plasticity, 2019, 119: 156−170.

[121] SONG K K, HAN X L, PAULY S, QIN Y S, KOSIBA K, PENG C X, GONG J H, CHEN P X, WANG L, SARAC B, KETOV S, MÜHLBACHER M, SPIECKERMANN F, KABAN I, ECKERT J. Rapid and partial crystallization to design ductile CuZr-based bulk metallic glass composites [J]. Materials & Design, 2018, 139: 132−140.

[122] SUN K, XU L M, WEBER H, WANG G, TSENG J C, SHEN J, WU S W, BIAN X L, KOSIBA K, KÜHN U, PAULY S. A refined local structure in a metallic glass tailored via flash-annealing [J]. Materials Characterization, 2021, 178: 111214.

[123] TU K N. Electromigration in stressed thin films [J]. Physical Review B, 1992, 45: 1409−1413.

[124] TAO C G, CULLEN W G, WILLIAMS E D. Visualizing the electron scattering force in nanostructures [J]. Science, 2010, 328: 736−740.

[125] TAKEMOTO R, NAGATA M, MIZUBAYASHI H. Effects of passing electric current on the elastic property of amorphous $Cu_{50}Zr_{50}$ and $Cu_{50}Ti_{50}$ [J]. Acta Materialia, 1996, 44: 2787−2795.

[126] YIU P, HSUEH C H, SHEK C H. Electroplastic forming in a Fe-based metallic glass ribbon [J]. Journal of Alloys and Compounds, 2016, 658: 795−799.

[127] YIU P, CHEN Y C, CHU J P, CHANG S Y, BEI H, JANG J S C, HSUEH C H. Rapid relaxation and embrittlement of Zr-based bulk metallic glasses by electropulsing [J]. Intermetallics, 2013, 34: 43−48.

[128] YIU P, HSUEH C H, SHEK C H. Rapid thermoplastic formation of Fe-based metallic glass foil achieved by electropulsing [J]. Materials Letters, 2014, 136: 353−355.

[129] KUMAR G, RECTOR D, CONNER R D, SCHROERS J. Embrittlement of Zr-based bulk metallic glasses [J]. Acta Materialia, 2009, 57: 3572−3583.

[130] SAMAVATIAN M, GHOLAMIPOUR R, AMADEH A A, SAMAVATIAN V. Inherent relation between atomic-level stresses and nanoscale heterogeneity in Zr-based bulk metallic glass under a rejuvenation process [J]. Physica B: Condensed Matter, 2020, 595: 412390.

[131] ZHANG Sai-long, SHI Bo, WANG Jin-hui, XU Yuan-li, JIN Pei-peng. Rejuvenation of a naturally aged bulk metallic glass by elastostatic loading [J]. Materials Science and Engineering: A, 2021, 806: 140843.

[132] ZHANG Sai-long, SHI Bo, WANG Jin-hui, JIN Pei-peng. Stress-induced gradient rejuvenation framework and memory effect in a metallic glass [J]. Scripta Materialia, 2022, 213: 114636.

[133] GU Ji, SONG Min, NI Song, LIAO Xiao-zhou, GUO Sheng-feng. Improving the plasticity of bulk metallic glasses via pre-compression below the yield stress [J]. Materials Science and Engineering: A, 2014, 602: 68−76.

[134] WANG Y M, ZHANG M, LIU L. Mechanical annealing in the homogeneous deformation of bulk metallic glass under elastostatic compression [J]. Scripta Materialia, 2015, 102: 67−70.

[135] DENG P, WANG X C, ZHANG F, QIN X M, GAO P, SUI Y D, TAN J. Effect of mechanical-annealing on the mechanical properties of a Zr-based bulk metallic glass [J]. International Journal of Modern Physics B, 2019, 33: 1940052.

[136] ZHANG M, WANG Y M, LI F X, JIANG S Q, LI M Z, LIU L. Mechanical relaxation-to-rejuvenation transition in a Zr-based bulk metallic glass [J]. Scientific Reports, 2017, 7: 625.

[137] CUI Jing-xian, LUO Qiang, DI Si-yi, ZHANG Zheng-guo, SHEN Bao-long. Rejuvenation-to-relaxation transition induced by elastostatic compression and its effect on deformation behavior in a Zr-based bulk metallic glass [J]. Metals, 2022, 12: 282.

[138] ZHANG L T, WANG Y J, PINEDA E, YANG Y, QIAO J C. Achieving structural rejuvenation in metallic glass by modulating β relaxation intensity via easy-to-operate mechanical cycling [J]. International Journal of Plasticity, 2022, 157: 103402.

[139] ZHANG Shu-han, WANG Xin-zhe, HAY J, SCHWARZ U D, DATYE A. Mechanical cycling-induced evolution of structure and local mechanical properties in a PdCuNiP bulk metallic glass [J]. Journal of Non-Crystalline Solids, 2024, 623: 122683.

[140] WANG X D, SONG S L, ZHU Z W, ZHANG H F, REN X C. Structural evolution under elastic cyclic loading in a Ti-based metallic glass [J]. Journal of Non-Crystalline Solids, 2022, 577: 121263.

[141] YE Y F, WANG S, FAN J, LIU C T, YANG Y. Atomistic mechanism of elastic softening in metallic glass under cyclic loading revealed by molecular dynamics simulations [J]. Intermetallics, 2016, 68: 5−10.

[142] LI Shuo, HUANG Ping, WANG Fei. Rejuvenation saturation upon cyclic elastic loading in metallic glass [J]. Computational Materials Science, 2019, 166: 318−325.

[143] WANG Peng, YANG Xin-hua. Atomistic investigation of aging and rejuvenation in CuZr metallic glass under cyclic loading [J]. Computational Materials Science, 2020, 185: 109965.

[144] LOU Y, XV S, LIU Z Y, MA J. Rejuvenation of Zr-based bulk metallic glasses by ultrasonic vibration-assisted elastic deformation [J]. Materials (Basel), 2020, 13: 4397.

[145] LOU Yan, LIU Xiao, YANG Xiao-le, GE Yang, ZHAO Dan-dan, WANG Hao, ZHANG Lai-chang, LIU Zhi-yuan. Fast rejuvenation in bulk metallic glass induced by ultrasonic vibration precompression [J]. Intermetallics, 2020, 118: 106687.

[146] LOU Yan, YANG Ling-yun, XV Shen-peng, MA Jiang. Fast increase in ductility and strength of Zr-based bulk amorphous alloys induced by intermittent high-frequency vibration loading [J]. Intermetallics, 2022, 142: 107467.

[147] WANG D P, YANG Y, NIU X R, LU J, YANG G N, WANG W H, LIU C T. Resonance ultrasonic actuation and local structural rejuvenation in metallic glasses [J]. Physical Review B, 2017, 95: 235407.

[148] CHEN Zhe, REN Shuai, ZHAO Rui, ZHU Jian, LI Xin,

ZHANG He-ting, LIN Hong-ji, ZHU Jia-hua, SOHRABI S, RUAN Wen-qing, MA Jiang. Plasticity and rejuvenation of aged metallic glasses by ultrasonic vibrations [J]. Journal of Materials Science & Technology, 2024, 181: 231−239.

[149] LI X, WEI D, ZHANG J Y, LIU X D, LI Z, WANG T Y, HE Q F, WANG Y J, MA J, WANG W H, YANG Y. Ultrasonic plasticity of metallic glass near room temperature [J]. Applied Materials Today, 2020, 21: 100866.

[150] ZHAI W, NIE L H, HUI X D, XIAO Y, WANG T, WEI B. Ultrasonic excitation induced nanocrystallization and toughening of $Zr_{46.75}Cu_{46.75}Al_{6.5}$ bulk metallic glass [J]. Journal of Materials Science & Technology, 2020, 45: 157−161.

[151] HUANG Hu, ZHANG Ji-liang, SHEK C H, YAN Ji-wang. Effects of pre-compression deformation on nanoindentation response of $Zr_{65}Cu_{15}Al_{10}Ni_{10}$ bulk metallic glass [J]. Journal of Alloys and Compounds, 2016, 674: 223−228.

[152] DING G, LI C, ZACCONE A, WANG W H, LEI H C, JIANG F, LING Z, JIANG M Q. Ultrafast extreme rejuvenation of metallic glasses by shock compression [J]. Science Advances, 2019, 5: eaaw6249.

[153] JOO S H, PI D H, SETYAWAN A D H, KATO H, JANECEK M, KIM Y C, LEE S, KIM H S. Work-hardening induced tensile ductility of bulk metallic glasses via high-pressure torsion [J]. Scientific Reports, 2015, 5: 9660.

[154] LI X X, WANG J G, KE H B, YANG C, WANG W H. Extreme rejuvenation and superior stability in a metallic glass [J]. Materials Today Physics, 2022, 27: 100782.

[155] QIU X B, BIAN X L, ŞOPU D, GAO Y X, YI J, JIA Y D, WANG G. Tunable rejuvenation behavior of a metallic glass by residual stress modulation [J]. Journal of Materials Research and Technology, 2023, 26: 8263−8271.

[156] WANG Z T, PAN J, LI Y, SCHUH C A. Densification and strain hardening of a metallic glass under tension at room temperature [J]. Physical Review Letters, 2013, 111: 135504.

[157] FU X L, TAN M J, WANG Y S, JARFORS A E W, GUPTA M. Deformation behavior of $Mg_{67}Zn_{28}Ca_5$ metallic glass at near supercooled liquid region [J]. Journal of Alloys and Compounds, 2013, 549: 100−104.

[158] WU J P, LIN Y, DUAN F H, CHEN Q, WANG H T, LI N, WEN J L, PAN J, LIU L. Unexpected creep behavior in a rejuvenated metallic glass [J]. Journal of Materials Science & Technology, 2023, 163: 140−149.

[159] DING Gan, JIANG Feng, SONG Xuan, DAI Lan-hong, JIANG Min-qiang. Unraveling the threshold stress of structural rejuvenation of metallic glasses via thermo-mechanical creep [J]. Science China Physics, Mechanics & Astronomy, 2022, 65: 264613.

[160] MIYAZAKI N, WAKEDA M, WANG Y J, OGATA S. Prediction of pressure-promoted thermal rejuvenation in metallic glasses [J]. NPJ Computational Materials, 2016, 2: 16013.

[161] DMOWSKI W, GIERLOTKA S, WANG Z, YOKOYAMA Y, PALOSZ B, EGAMI T. Pressure induced liquid-to-liquid transition in Zr-based supercooled melts and pressure quenched glasses [J]. Scientific Reports, 2017, 7: 6564.

[162] EBNER C, RAJAGOPALAN J, LEKKA C, RENTENBERGER C. Electron beam induced rejuvenation in a metallic glass film during in-situ TEM tensile straining [J]. Acta Materialia, 2019, 181: 148−159.

[163] LIU Ting-kun, GUO Wei, CRESPILLO M L, JIN Ke, ZHANG Yan-wen, BEI Hong-bin, GAO Yan-fei. Indirectly probing the structural change in ion-irradiated Zr-based metallic glasses from small scale mechanical tests [J]. Intermetallics, 2020, 121: 106794.

[164] KHADEMOREZAIAN S, TOMUT M, PETERLECHNER M, DA SILVA PINTO M W, RÖSNER H, DIVINSKI S, WILDE G. Extreme rejuvenation of a bulk metallic glass at the nanoscale by swift heavy ion irradiation [J]. Journal of Alloys and Compounds, 2024, 980: 173571.

[165] WANG Peng-wei, LI Ming-fei, MALOMO B, YANG Liang. Neutron irradiation-induced rejuvenation in ZrCu metallic glass [J]. Journal of Materials Science, 2022, 57: 12642−12652.

[166] BRECHTL J, WANG H, KUMAR N A P K, YANG T, LIN Y R, BEI H, NEUEFEIND J, DMOWSKI W, ZINKLE S J. Investigation of the thermal and neutron irradiation response of BAM-11 bulk metallic glass [J]. Journal of Nuclear Materials, 2019, 526: 151771.

[167] CHEN T C, RAYA I, SHAFIK S S, JABBAR A H, TUMANOV D, SURENDAR A, SEVBITOV A, HOI H T, MUSTAFA Y F, VLADIMIROVICH K O, KADHIM M M, SAJJADIFAR S, REPNIKOV N I. Role of thermal history on atomic structure and ductility of ion-irradiated metallic glasses [J]. Modelling and Simulation in Materials Science and Engineering, 2021, 30: 025002.

[168] RAGHAVAN R, BOOPATHY K, GHISLENI R, POUCHON M A, RAMAMURTY U, MICHLER J. Ion irradiation enhances the mechanical performance of metallic glasses [J]. Scripta Materialia, 2010, 62: 462−465.

[169] RAGHAVAN R, KOMBAIAH B, DÖBELI M, ERNI R, RAMAMURTY U, MICHLER J. Nanoindentation response of an ion irradiated Zr-based bulk metallic glass [J]. Materials Science and Engineering: A, 2012, 532: 407−413.

[170] LI Na, ZHANG Xiao-nan, ZHANG Li-song, ZHANG Peng, MEI Xian-xiu, QIANG Jian-bing, WANG You-nian. Effects of He ion irradiation on the structural stability and deformation behavior in $Zr_{63.5}Cu_{23}Al_9Fe_{4.5}$ and $Fe_{80}B_{13}Si_7$ metallic glasses [J]. Journal of Non-Crystalline Solids, 2023, 616: 122474.

[171] AVCHACIOV K A, RITTER Y, DJURABEKOVA F, NORDLUND K, ALBE K. Effect of ion irradiation on structural properties of $Cu_{64}Zr_{36}$ metallic glass [J]. Nuclear Instruments and Methods in Physics Research: Section B, 2014, 341: 22−26.

[172] QIU Y H, XU C, FU E G, WANG P P, DU J L, HU Z Y, YAN X Q, CAO X Z, WANG Y G, SHAO L. Mechanisms for the free volume tuning the mechanical properties of metallic glass through ion irradiation [J]. Intermetallics, 2018, 101: 173−178.

[173] TANG Y, ZHOU H, LU H, WANG X, CAO Q, ZHANG D, YANG W, JIANG J Z. Extra plasticity governed by shear band deflection in gradient metallic glasses [J]. Nature Communications, 2022, 13: 2120.

[174] RYU W, YAMADA R, SAIDA J. Tailored hardening of ZrCuAl bulk metallic glass induced by 2D gradient

rejuvenation [J]. NPG Asia Materials, 2020, 12: 52.
[175] WANG Q, YANG Y, JIANG H, LIU C T, RUAN H H, LU J. Superior tensile ductility in bulk metallic glass with gradient amorphous structure [J]. Scientific Reports, 2014, 4: 4757.
[176] ZHAO L, CHAN K C, CHEN S H, FENG S D, HAN D X, WANG G. Tunable tensile ductility of metallic glasses with partially rejuvenated amorphous structures [J]. Acta Materialia, 2019, 169: 122−134.
[177] WANG Yong-wei, LI Mo, XU Jin-wu. Free volume gradient effect on mechanical properties of metallic glasses [J]. Scripta Materialia, 2017, 130: 12−16.
[178] VARGONEN M, HUANG Li-ping, SHI Yun-feng. Evaluating Mohr−Coulomb yield criterion for plastic flow in model metallic glasses [J]. Journal of Non-Crystalline Solids, 2012, 358: 3488−3494.

通过回春提高金属玻璃的塑性：综述

董 权[1]，李才巨[2]，Baran SARAC[3]，Jürgen ECKERT[3,4]，谭 军[1]

1. 重庆大学 材料科学与工程学院，重庆 400044；
2. 昆明理工大学 材料科学与工程学院，昆明 650093；
3. Erich Schmid Institute of Materials Science, Austrian Academy of Sciences, Jahnstraße 12, A-8700, Leoben, Austria;
4. Department of Materials Science, Chair of Materials Physics, Montanuniversität Leoben, Jahnstraße 12, A-8700, Leoben, Austria

摘 要：近年来，通过回春处理调整金属玻璃的内部结构并增强其塑性已成为人们关注的焦点。本文全面综述了在金属玻璃中诱导回春的各类方法及其内在机制，包括深冷循环处理和退火诱导回春的热激活法、机械驱动的预弹性加载法和塑性变形法、热−机械耦合的热机械蠕变和热塑性变形法以及辐照诱导的回春。此外，还探讨了通过梯度回春促进自由体积梯度分布，诱导剪切带偏转从而增强塑性的策略。最后，本文深入探讨了在室温条件下开发高塑性金属玻璃所面临的挑战与前景。本综述有望为系统理解通过回春处理来提升金属玻璃塑性的手段及其机制提供参考。

关键词：金属玻璃；塑性；回春；自由体积；剪切带

(Edited by Xiang-qun LI)